## Title

PHOTOIONTZATION OF HELIUM ABOVE THE He+ (n=2) THRESHOLD: AUTOIONIZATION AND FINAL-STATE SYMMETRY



## Author

Lindle, D.W.

## Publication Date

1983-06-01

# Lawrence Berkeley Laboratory
UNIVERSITY OF CALIFORNIA

## Materials & Molecular Research Division



Submitted to Physical Review A

PHOTOIONIZATION OF HELIUM ABOVE THE $He^+(n=2)$ THRESHOLD: AUTOIONIZATION AND FINAL-STATE SYMMETRY

D.W. Lindle, T.A. Ferrett, U. Becker, P.H. Kobrin,
C.M. Truesdale, H.G. Kerkhoff, and D.A. Shirley

June 1983



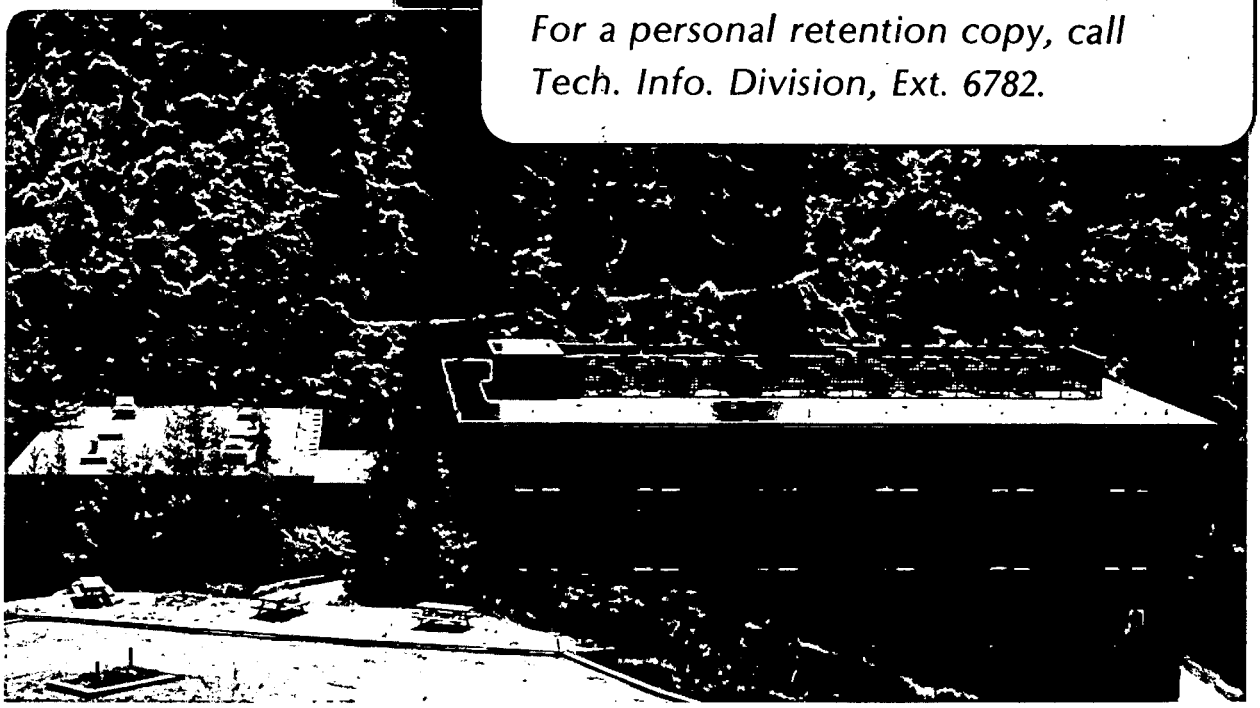

Prepared for the U.S. Department of Energy under Contract DE-AC03-76SF00098

## DISCLAIMER

LBL-15094

# PHOTOIONIZATION OF HELIUM ABOVE THE $He^+(n=2)$ THRESHOLD: AUTOIONIZATION AND FINAL-STATE SYMMETRY

D. W. Lindle, T. A. Ferrett, U. Becker,* P. H. Kobrin,†

C. M. Truesdale,‡ H. G. Kerkhoff,* and D. A. Shirley

Materials and Molecular Research Division
Lawrence Berkeley Laboratory
and
Department of Chemistry
University of California
Berkeley, California 94720

*Permanent address: Technische Universität Berlin, Fachbereich Physik, 1000 Berlin 12, West Germany.
†Present address: Department of Chemistry, Pennsylvania State University, University Park, PA 16802.
‡Present address: Corning Glass Works, Corning, NY 14831.

# PHOTOIONIZATION OF HELIUM ABOVE THE $He^+(n=2)$ THRESHOLD: AUTOIONIZATION AND FINAL-STATE SYMMETRY

D. W. Lindle, T. A. Ferrett, U. Becker,* P. H. Kobrin,†
C. M. Truesdale,‡ H. G. Kerkhoff,* and D. A. Shirley

Materials and Molecular Research Division
Lawrence Berkeley Laboratory
and
Department of Chemistry
University of California
Berkeley, California 94720

The energy dependences of the partial cross section, $\sigma_{n=2}$, the satellite branching ratio, $R_{21}$, and the angular distribution asymmetry parameter, $\beta_{n=2}$, for simultaneous photoionization and photoexcitation to the n=2 states of $He^+$ have been measured in the range 67.5 eV $\leq h\nu \leq$ 90 eV. In the non-resonance regions (67.5 eV $\leq h\nu \leq$ 69.5 eV and 75 eV $\leq h\nu \leq$ 90 eV), the measured $\beta_{n=2}$ values and theoretical values of $\beta_{2s}$ and $\beta_{2p}$ have been used to determine the ratio of the 2p photoionization cross section to the 2s photoionization cross section. These results indicate that the $He^+(n=2)$ satellite is predominantly 2p near threshold, in agreement with the other experimental and most of the theoretical results reported to date. In the resonance region leading to the n=3 threshold (69.5 eV $\leq h\nu \leq$ 73.0 eV), the effects of a series of autoionizing Rydberg levels on $\sigma_{n=2}$ and $\beta_{n=2}$ have been measured, this being the first detailed measurement of the angular distribution of a satellite

over an autoionization resonance. In addition, the total cross section and the 1s partial cross section have been measured for the first member of this series (3s3p). The total cross-section data were found to disagree with all previous experimental and theoretical results. Parameters defining all of the measured resonance profiles are presented.

*Permanent address: Technische Universität Berlin, Fachbereich Physik, 1000 Berlin 12, West Germany.
†Present address: Department of Chemistry, Pennsylvania State University, University Park, PA 16802.
‡Present address: Corning Glass Works, Corning, NY 14831.

## I. Introduction

The photoionization of helium provides the simplest example of electron correlation in atomic physics. Because correlation cannot occur in the hydrogen-like final state, theoretical studies of initial-state and continuum-state correlation effects are easier to interpret for the photoionization process. For this reason, helium is an important system for testing various theoretical approaches to the phenomenon of electron correlation. Past interest focused upon absolute cross-section measurements, as reviewed by Marr and West.[1] Theoretical calculations[2] of the total cross section, at least below the $He^+(n=2)$ threshold, have proven to be very accurate. Recent interest[3-10] has centered upon the photoionization processes above this threshold, which can leave the residual $He^+$ ion in the 2s or 2p excited states. Several calculations[11-17] of the partial photoionization cross section, the satellite and subshell branching ratios, and the angular distribution asymmetry parameter have been performed for the $He^+(n=2)$ states, indicating that much is still to be learned from this simple system about the influence of correlation on measurable quantities.

Figure 1 depicts the atomic and ionic states in helium relevant to this experiment. We have studied the photoionization processes

$$He(1s^2) + h\nu \rightarrow He^+(1s,2s,2p) + e^- \qquad (1)$$

as a function of photon energy and photoelectron ejection angle. The $He^+(2s)$ and $He^+(2p)$ states are effectively degenerate in a photoemission experiment, and thus comprise a single satellite line, which we designate $He^+(n=2)$. We have measured the partial cross sections, $\sigma$, and angular distribution asymmetry parameters, $\beta$, for the processes represented in Eq. (1) that leave the $He^+$ ion in the 1s or the n=2 final states, as well as the branching ratio, $R_{21} = \sigma_{n=2}/\sigma_{1s}$, of the satellite intensity relative to that of the main line. The threshold for production of the n=2 states from the ground state of the helium atom is 65.4 eV. We have taken photoelectron spectra for photon energies from 1.9 eV above this threshold to $h\nu$ = 90 eV. This energy range can be divided into resonance and non-resonance regions. In the resonance region (69.5 eV $\leq h\nu \leq$ 73.0 eV), it is possible to excite a series of Rydberg levels leading to the third ionization threshold at 73.0 eV, with subsequent autoionization.

The non-resonance data, taken with photon energies in the ranges 67.5 eV $\leq h\nu \leq$ 69.5 eV and 75 eV $\leq h\nu \leq$ 90 eV, show good agreement with previous measurements[3-6,8,10] and calculations[11-17] of the partial cross sections for both the n=1 and n=2 final states (processes DI in Fig. 1) and for the total (i.e. 2s plus 2p) satellite branching ratio. The ratio of the 2p cross section to the 2s cross section, R, which can be derived from $\beta_{n=2}$, provides a more sensitive test of theory. Discrepancies exist among the various experimental[7-10] and theoretical[12-17] values of R reported to date. Chang[14] has predicted that near threshold the 2s contribution to $\sigma_{n=2}$ is larger than that of

the 2p level, in contrast to several other predictions.[12,13,15-17] Experimentally, the photoemission data of Bizau et. al.[7] tend to support Chang's calculation, but other photoemission[9,10] and fluorescence[8] experiments do not. Our results support the conclusion that the $He^+(n=2)$ final state is predominantly 2p near threshold. This disagreement in the theoretical results indicates the need for a better understanding of the contributions of electron correlation to the photoionization process.

A different perspective on correlation can be obtained in the analysis of autoionization resonances. The interaction of various continuum-state wavefunctions with an excited Rydberg level determines the extent and profile of the autoionization process. We have taken photoelectron spectra in the region of the lowest four Rydberg levels leading to the $He^+(n=3)$ ionization threshold at 73.0 eV. The four levels studied are shown in the left-hand portion of Fig. 1. Large variations in $\sigma_{n=2}$ and $\beta_{n=2}$ were found at these resonances. The partial cross section of the main line, $\sigma_{1s}$, was also affected by approximately the same magnitude as the satellite partial cross section, but proportionately this effect was much smaller. Our measured variation in $\sigma_{n=2}$ agrees with the fluorescence data of Woodruff and Samson.[8] The detailed variation of $\beta_{n=2}$ over the autoionization resonances is presented here for the first time. In addition, our measurements of the total cross section over the first member of this Rydberg series differ quite markedly with the previous experimental[18] and theoretical[19,20] results.

The experimental procedures are described in Section II. The non-resonance data are presented in Section III, and the behavior of the cross sections, branching ratios and asymmetry parameters over the autoionization resonances is discussed in Section IV. Conclusions are presented in Section V.

## II. Experimental

Synchrotron radiation from the new 4° 'grasshopper' monochromator at the Stanford Synchrotron Radiation Laboratory (SSRL) was used to photoionize an effusive beam of helium atoms. The photoelectrons were detected at 0° and 54.7° with respect to the polarization vector of the photon beam by the double-angle time-of-flight (DATOF) method,[21] taking advantage of the pulsed time structure of the synchrotron radiation from the SPEAR storage ring. This configuration allowed us to measure simultaneously the partial cross sections and angular distribution asymmetry parameters for both the main and satellite lines of $He^+$.

The DATOF photoelectron spectrometer has been described previously.[22] It is ideally suited for studying low cross section satellite lines, such as in helium, because of its high signal-to-noise ratio and its ability to collect nearly all photoelectron energies simultaneously. The experimental chamber was isolated from the monochromator vacuum of $\sim 10^{-10}$ torr by a 1500Å thick aluminum window. The typical chamber pressure was $3\text{-}4 \times 10^{-3}$ torr. For partial cross-section measurements, the sample pressure was monitored by a capacitance manometer and the photon flux by a sodium salicylate scintillator and an optical photomultiplier tube (RCA 8850). Calibration of the analyzers was accomplished by the measurement of the known partial cross sections and asymmetry parameters of the 2s and 2p levels of $Ne^+$. Typical count rates for the $He^+(n=2)$ satellite were

3-8 per second, with accumulation times of 1000 seconds for each spectrum. An example of a time-of-flight spectrum for helium from the 0° detector is shown in Fig. 2.

The angular distribution of photoelectrons ejected from a randomly-oriented sample by linearly-polarized radiation, in the dipole approximation, is given by

$$\frac{d\sigma(E,\theta)}{d\Omega} = \frac{\sigma(E)}{4\pi} [1 + \beta(E)P_2(\cos\theta)] \quad , \qquad (2)$$

where E is the photon energy, $\theta$ is the angle between the propagation vector of the photoelectron and the polarization vector of the ionizing radiation, $\beta(E)$ is the asymmetry parameter that completely describes the angular distribution, and $P_2(\cos\theta)$ is the second Legendre polynomial. Photoelectron intensities measured at $\theta = 54.7°$ (where $P_2(\cos\theta) = 0$) are directly proportional to $\sigma(E)$. The measurement of photoelectron intensities at one additional angle suffices to determine $\beta(E)$. Throughout the remainder of this paper, explicit expression of the dependence of $\sigma$ and $\beta$ on the photon energy has been omitted for clarity.

## III. Non-Resonance Photoionization

Our measurement of the branching ratio $R_{21}$ is shown in Fig. 3, along with several theoretical curves and other experimental measurements. The present results show excellent agreement with the previous measurements.[3,4,6] We see, also, that the available theoretical calculations[11-15,17] agree reasonably well with one another and predict the branching ratio to within ~25%. The absolute partial cross section of the n=2 satellite is also predicted well by these same calculations. We do not show our relative partial cross sections for the n=2 or 1s levels, but note that they also agree with the previous measurements. The ability to predict the energy dependence of $R_{21}$ appears to be nearly independent of the degree of configuration interaction (CI) included in the calculations.

This is not true, however, when the individual partial cross sections for the 2s and 2p final states are considered. The measurement of these partial cross sections, or their ratio, is a more sensitive test of the theoretical calculations, because the energy dependences of $\sigma_{2s}$ and $\sigma_{2p}$ are quite different. The reasons for these differences can be understood from a discussion of CI as it pertains to helium photoionization.

For the case that CI is only important in the initial (eigen) state of the helium atom (ISCI), the initial state is properly written as an admixture of the $1s^2$, $2s^2$, $2p^2$ and higher configurations. The

ground state is predominantly $1s^2$. If we consider then that the $1s^2$, $2s^2$, $2p^2$, etc. configurations are not eigenstates (i.e. they are not orthogonal to each other), then the degree to which any one of the other configurations mixes into the ground state can be estimated by considering its overlap with the $1s^2$ configuration. This estimate suggests that $2s^2$ plays a more important role in ISCI than does $2p^2$. Furthermore, if we assume that ionization from either the $2s^2$ or the $2p^2$ configuration is equally probable, then the partial cross sections for the production of the 2s and 2p final states (by ionization from the $2s^2$ or $2p^2$ configuration, respectively) is dependent only on the mixing coefficients of $2s^2$ and $2p^2$ in the initial state. Therefore, we expect ISCI to lead to a predominance of $He^+(2s)$. We also can see that this result is valid for all photoelectron energies because the ISCI mixing coefficients are independent of energy. Thus, if CI were to occur only in the initial state, then the ratio R will be constant and less than unity.

However, the effects of CI in the continuum state (CSCI) must also be considered. The continuum state includes both the ionic core left after photoionization and the photoelectron. For simplicity in this discussion, we will consider the initial state to be completely $1s^2$. Configuration interaction in the continuum thus constitutes mixing of configurations such as $2s\varepsilon p$ and $2p\varepsilon s$ with $1s\varepsilon p$. Again, we estimate the degree of mixing by examining the overlap of a given configuration with $1s\varepsilon p$. Because the photoelectron is included in these wavefunctions, we can expect the mixing coefficients, and hence the 2s and 2p cross

sections, to be energy dependent. Because of the nature of continuum wavefunctions at low energy, the overlap between $2p\varepsilon s$ and $1s\varepsilon p$ (which can be determined from $\langle 1s|\varepsilon s\rangle$ and $\langle 2p|\varepsilon p\rangle$) is large near threshold, and quickly diminishes with increasing energy. The overlap between $2s\varepsilon p$ and $1s\varepsilon p$ will not be strongly energy dependent, because of the similarity of the continuum part of these two configurations. The result of CSCI would then likely be a predominance of the 2p final state near threshold, this predominance decreasing as the energy increases. This discussion of CSCI is oversimplified to the extent that we have ignored the near degeneracy of the 2s and 2p final states. Their proximity in energy allows them to be strongly coupled in the continuum state. Despite this complication, we expect the conclusions to be qualitatively correct.

To understand the complete picture for helium photoionization, it is necessary to combine the effects of ISCI and CSCI discussed above. Configuration interaction in the hydrogen-like final state is not possible, and does not need to be considered. Qualitatively, we conclude that at threshold the 2p final state will be maximally produced and may be more likely than the 2s final state, whereas in the high-energy limit, the 2s final state will be most important. At some intermediate energies, both final states will be equally important, and we can expect strong coupling between them. Similar conclusions can be derived from a different argument using shake theory.[15] Quantitatively, the degree of predominance of one final state over the other and the applicable energy ranges can only be determined by theoretical

calculations that accurately treat the effects of ISCI and CSCI. Comparison of such calculations with experimental results can yield information about the type and degree of CI present in the helium system, as well as important results concerning what treatments of CI are most accurate.

Experimentally, two approaches have been taken. Woodruff and Samson[8] measured R directly by taking advantage of the long lifetime of $He^+(2s)$ to distinguish between fluorescence from the 2s and 2p levels. A second method, used by several groups,[7,9,10] including ours, relies on the measurement of the angular distribution asymmetry parameter, $\beta_{n=2}$, which is a weighted average of $\beta_{2s}$ and $\beta_{2p}$:

$$\beta_{n=2} = \frac{\sigma_{2s}\beta_{2s} + \sigma_{2p}\beta_{2p}}{\sigma_{2s} + \sigma_{2p}} \quad . \tag{3}$$

By rearranging Eq. (3), and using the fact that $\beta_{2s}$ is always 2, R can be expressed in terms of $\beta_{n=2}$:

$$R = \frac{\sigma_{2p}}{\sigma_{2s}} = \frac{2 - \beta_{n=2}}{\beta_{n=2} - \beta_{2p}} \quad . \tag{4}$$

This latter approach, of course, must rely on the calculated values of $\beta_{2p}$. Fortunately, the two available calculations[7,13] of $\beta_{2p}$ agree rather well.

Our results for $\beta_{n=2}$ are presented in Fig. 4 along with the other experimental results[7,9,10] for $\beta_{n=2}$ and theoretical calculations[7,13] of $\beta_{n=2}$ and $\beta_{2p}$. Agreement among the experiments is excellent throughout the energy range shown. The region between 70 and 75 eV is blank

because of the presence of several strong autoionizing resonances (see Section IV). Figure 5 shows the values of R derived from the experimental data in Fig. 4 and the calculated values of $\beta_{2p}$ from Jacobs and Burke.[13] Also shown are five calculations[12-17] of this ratio and the direct measurements of R by Woodruff and Samson.

The strong energy dependence of R below 100 eV can be understood from the above discussion of ISCI and CSCI. Because CSCI is more important at lower energies, we expect $\sigma_{2p}$ to make a stronger contribution to $\sigma_{n=2}$ near threshold, as confirmed by the data. Also, since ISCI is nearly energy-independent, we expect the ratio $\sigma_{2s}/\sigma_{1s}$ to be fairly constant for all photon energies. Direct measurements[8] of $\sigma_{2s}$ support this conclusion about $\sigma_{2s}/\sigma_{1s}$ for the first 60 eV above threshold. At the high-energy limit the n=2 peak should be mostly 2s, though no experimental confirmation is available. The satellite branching ratio, $R_{21}$, in this limit has been calculated[11,13] to be 4.8%, which can be compared to the value of 6% from the highest-energy measurements (~190 eV) to date.[4]

The theories used in the calculation of R differ significantly in sophistication. The calculation of Richards and Larkins[15,17] used Hartree-Fock (HF) wavefunctions in which the effects of relaxation have been included, but not CI. The calculation by Chang[14] also used HF wavefunctions, but included CI in both the initial state and the continuum states. Jacobs[12] and Jacobs and Burke[13] used a 56-term Hylleras initial-state wavefunction, which is a nearly exact approximation of the He($1s^2$) ground state, and a close-coupling

calculation for the final state, which is similar to CSCI. The latest calculation by Berrington et al.[16] is an improvement on the earlier close-coupling calculations in which care was taken to use the same configurations in the expansions for both the initial and continuum states. All of the calculations used final-state wavefunctions that are purely hydrogenic.

Above 85 eV, all of the calculations show the same behavior and they all agree with experiment to within the errors. Below 85 eV, however, Chang's curve deviates significantly from the rest and predicts a predominance of 2s near threshold. The experimental results show clearly that this is not correct, and we conclude that the 2p final state is the major component of $He^+(n=2)$ at threshold, being more than twice as likely as the 2s final state. The calculation of Berrington et al. shows the best overall agreement with the present results.

The three close-coupling calculations (Jacobs, Jacobs and Burke and Berrington et al.) and the calculation of Richards and Larkins behave similarly at low energy, despite the fact that the latter is a much less sophisticated calculation. Richards and Larkins have concluded that CI and exchange are unimportant to their calculation except near threshold, and they cite this as the reason their calculation does so well. Furthermore, they suggest[23] that the discrepancy in Chang's calculation may be the result of the use of CI wavefunctions that do not accurately take into account the direct interaction of the outgoing channels, which the other calculations

do.[12,13,16] This may ultimately be the result of cancellation between large terms in the calculation of the transition amplitude.[14]

This example illustrates that much is still to be learned about the effects of CI on the calculation of the energy dependence of satellite cross sections. Except for isolated calculations on the Ne K-shell,[24] the Li K-shell,[15,17] and the valence shell of Fe,[25] the helium calculations are the only such theoretical studies completed to date. Helium thus appears to be a good candidate for further studies of electron-correlation effects in atomic photoionization.

At the photon energy of 80 eV (see Fig. 2), we were able to detect photoelectrons from the $He^+(n=3)$ final state. We determine its branching ratio relative to the main line, $R_{31}$, to be $1.8 \pm 0.2\%$ and its asymmetry parameter to be $-0.2 \pm 0.2$. This value for $R_{31}$ is in agreement with previous estimates[6,15,26] at this energy and the data of Bizau et al.[27] The negative value for $\beta_{n=3}$ indicates that the 3s final state is not the major component of this peak. In fact, $\sigma_{3p}/\sigma_{3s}$ must be greater than 2 at 80 eV if the $He^+(3d)$ final state has a negligible contribution, as predicted by Richards.[15]

## IV. Resonance Photoionization

Madden and Codling[28] first observed the Rydberg levels leading to the n=3 ionization threshold in helium in the energy range $69.5 \leq h\nu \leq 73.0$ eV. Of the five possible Rydberg series in this region, only one has been found to be significant. It is designated (sp, 3n+) $^1P^\circ$, which is a positive admixture of 3snp $^1P^\circ$ and 3pns $^1P^\circ$. It has also been given[29] the notation $1_n$, which we shall use here except when the $1_3$ resonance is discussed alone: then we shall refer to it as the 3s3p resonance. The (sp, 3n−) $^1P^\circ$ (or $-1_n$) series, the negative admixture of 3snp $^1P^\circ$ and 3pns $^1P^\circ$, has also been observed, but it is small enough to be neglected in the present analysis. The other possible $^1P^\circ$ series (with major component 3pnd, 3dnp or 3dnf) have not been observed. To discuss the effects of the first four members of the $1_n$ series on the photoionization of helium, a summary of several theoretical descriptions of autoionization is necessary.

### A. Theoretical Background

The effect of an isolated resonance, such as a Rydberg level, on the total photoabsorption or total photoionization cross section was originally derived by Fano.[30] The presence of a discrete level embedded in one or more continua causes an interference in the photon absorption process because of the indistinguishability of the two

pathways, direct ionization and autoionization, leading to the final state. Fano derived the following expression for the total cross section, $\sigma_t$, for the case of a single discrete state interacting with one or more continuum states:

$$\sigma_t = \sigma_0 \left[ \rho^2 \frac{(q + \varepsilon)^2}{1 + \varepsilon^2} + 1 - \rho^2 \right] , \tag{5a}$$

$$\varepsilon = \frac{E - E_0}{\Gamma/2} , \tag{5b}$$

where the Fano parameters q and $\rho^2$ are assumed constant over the resonance, $\sigma_0$ is the cross section far from the resonance, $\Gamma$ and $E_0$ are the full-width at half-maximum (FWHM) and the position of the resonance, respectively, and $\varepsilon$ is a reduced energy.

The quantities q, $\rho^2$, $\sigma_0$ and $\Gamma$ can all be expressed in terms of the dipole matrix elements for transitions from the ground state, g, to the discrete state, $\phi$, and to the continua, $\mu$, togther with the Coulomb interaction matrix elements coupling the discrete state to the continua. The q parameter, which governs the shape of the total cross section, is given by

$$q = \frac{\langle \Phi | \vec{r} | g \rangle}{\pi \sum_{\mu} \langle \phi | V | \mu \rangle \langle \mu | \vec{r} | g \rangle} , \tag{6}$$

and the correlation coefficient, $\rho^2$, which is a measure of the strength of the resonance, is given by

$$\rho^2 = \frac{\sum_{\mu} |\langle \phi | V | \mu \rangle \langle \mu | \vec{r} | g \rangle|^2}{\sum_{\mu} |\langle \phi | V | \mu \rangle|^2 \sum_{\mu} |\langle \mu | \vec{r} | g \rangle|^2} , \tag{7}$$

where $\vec{r}$ and V represent the dipole and Coulomb operators, respectively, and $\Phi$ is the discrete state modified by an admixture of the continuum states. The degree to which $\Phi$ is different from $\phi$ is dependent upon the energy variations of the continuum wavefunctions in the vicinity of the resonance. The linewidth of the resonance is given by

$$\Gamma = 2\pi \sum_{\mu} |\langle \phi | V | \mu \rangle|^2 , \tag{8}$$

and the non-resonance, background cross section is given by

$$\sigma_0 = \sum_{\mu} |\langle \mu | \vec{r} | g \rangle|^2 . \tag{9}$$

While the matrix elements in Eqs. (6) and (7) are not strictly energy-independent, they are slowly-varying functions of energy, and q and $\rho^2$ are therefore assumed to be constant over the energy range of the resonance.

The Fano parametrization [Eqs. (5)-(9)] can explain the many different shapes measured for autoionization resonances. For example, the sign of the q parameter determines whether the resonance profile of the total cross section reaches its minimum on the low-energy side ($q > 0$) or the high-energy side ($q < 0$) of the resonance. This property will be referred to as the 'phase' of the resonance profile. Other shapes can also be obtained from these expressions, such as a

window resonance ($q = 0$) or a non-interfering Lorentzian peak added to the background cross section ($|q| \gg 0$).

The parametrization shown above is most applicable to the effect of an isolated resonance on the total photoabsorption cross section. In general, however, atomic Rydberg levels form a series whose members are not well-separated in energy and thus cannot be considered isolated. Equation (5a) is not easily adaptable to such a series of non-interacting, closely-spaced resonances because the background cross section appears as a multiplicative factor for each resonance, making a simple summation unsatisfactory. Shore[31] has derived an equivalent expression that is better suited for a series of closely-spaced resonances because it is mathematically simpler to work with. His expression is

$$\sigma_t = C + \sum_k \frac{B_k + A_k \epsilon_k}{1 + \epsilon_k^2} , \qquad (10)$$

where C is the background cross section for the series of resonances, the summation is over the k resonances, $\epsilon_k$ is as defined in Eq. (5b) for each resonance, and $A_k$ and $B_k$ are the shape parameters for the kth resonance, which we shall refer to as the "Shore parameters". The value C is understood to be a slowly-varying function of the photon energy. As with the Fano parameters, q and $\rho^2$, the Shore parameters, A and B, are assumed constant in the resonance region.

It is clear that for the case of a single, isolated resonance, the Fano and Shore parametrizations can be expressed in the same

mathematical form, as follows:

$$\sigma_t = \sigma_0 \left[ \frac{C_1 + C_2\varepsilon + \varepsilon^2}{1 + \varepsilon^2} \right] , \tag{11}$$

where $C_1$ and $C_2$ can be expressed in terms of either q and $\rho^2$ or A and B. We note that although the Shore formalism is to be preferred for multiple resonances, the parameters A and B are not dimensionless quantities as are q and $\rho^2$. Because of this, the Fano formalism is more descriptive in the isolated-resonance case.

The formalisms presented so far were derived for the total cross section. In a photoemission experiment, however, partial cross sections are commonly measured. Starace[32] has addressed the problem of several outgoing channels in the vicinity of an autoionization resonance. Davis and Feldkamp[33] and Combet Farnoux[34] have derived equivalent expressions. We shall use the notation of Starace. His expression for the partial cross section of each of the observable photoemission channels, $\mu$, is

$$\sigma(\mu) = \frac{\sigma_0(\mu)}{1 + \varepsilon^2} \left[ \varepsilon^2 + 2\left\{ q\mathrm{Re}(\alpha_\mu) - \mathrm{Im}(\alpha_\mu) \right\}\varepsilon + 1 \right.$$
$$\left. - 2q\mathrm{Im}(\alpha_\mu) - 2\mathrm{Re}(\alpha_\mu) + (q^2 + 1)|\alpha_\mu|^2 \right] , \tag{12}$$

where $\sigma_0(\mu)$ is the off-resonance partial cross section for the $\mu$th observable final state and $\varepsilon$ and q are defined in Eqs. (5b) and (6), respectively. The complex parameter, $\alpha_\mu$, is given by[35]

$$\alpha_\mu = \frac{\langle \phi | V | \mu \rangle}{\langle g | \vec{r} | \mu \rangle} \quad \frac{2\pi}{\Gamma} \sum_\mu \langle g | \vec{r} | \mu \rangle \langle \mu | V | \phi \rangle \quad , \tag{13}$$

with $\Gamma$ given by Eq. (8). The term in brackets is common to all channels. The $\alpha_\mu$-parameters can be thought of as replacing $\rho^2$ as the correlation coefficient for each channel when partial cross sections are measured. It is important to note that each $\mu$ represents an observable photoionization channel (eg. $He^+(1s\varepsilon p_{1/2})$). This restriction was not necessary in the Fano and Shore derivations of the resonance behavior of the total cross section, because the individual photoemission channels only appeared in summations over $\mu$. It is clear that Eq. (12) has the same form as Eq. (11), because it describes the characteristic behavior of a cross section in the vicinity of an autoionization resonance. We will refer to $C_1(\mu)$ and $C_2(\mu)$ as the "Starace parameters". Because all of the preceding formalisms, whether for total or partial cross sections, have the same mathematical form, it is possible to equate the parameters of the various formalisms, keeping in mind that expression of the parameters in terms of the appropriate matrix elements is only possible if the proper formalism for any given experiment is used. For example, although effective Fano prameters can be derived for the autoionization profile of a partial cross section, it is misleading to report them as the appropriate resonance parameters, because the expressions given by Fano for q and $\rho^2$ are not directly applicable to a partial cross section. They can be used in a descriptive context, however. This point will be discussed further in the next section.

An additional complication, discussed in Ref. (36), occurs because every peak, m, in a photoemission spectrum contains more than one of the channels, $\mu$, such as the $He^+(1s)$ peak, which has contributions from two outgoing channels; $1s\varepsilon p_{1/2}$ and $1s\varepsilon p_{3/2}$. Thus, the partial cross section for each photoelectron peak, $\sigma(m)$, is the sum of several $\sigma(\mu)$. The expression for $\sigma(m)$ is of the same form as Eq. (12), but with $\sigma_0(\mu)$ replaced by the off-resonance partial cross section for the unresolved channels, $\sigma_0(m)$, and $Re(\alpha_\mu)$, $Im(\alpha_\mu)$ and $|\alpha_\mu|^2$ replaced by $Re\langle\alpha\rangle_m$, $Im\langle\alpha\rangle_m$ and $\langle|\alpha|^2\rangle_m$, which are averaged quantities weighted by the $\sigma_0(\mu)$. The Schwartz inequality requires that

$$(Re\langle\alpha\rangle_m)^2 + (Im\langle\alpha\rangle_m)^2 \leq \langle|\alpha|^2\rangle_m \quad , \tag{14}$$

so that the modified Eq. (12) contains three unknown quantities. Because a fit to the form of Eq. (11) only provides two parameters, it is, in general, impossible to solve for all three unknowns.

The angular distribution asymmetry parameter, $\beta$, can also show effects of autoionization. Kabachnik and Sazhina[37] have shown that, for photoionization in the region of an isolated resonance, $\beta$ is given by

$$\beta = \frac{X'\varepsilon^2 + Y'\varepsilon + Z'}{A'\varepsilon^2 + B'\varepsilon + C'} \quad , \tag{15}$$

where A', B' and C' are defined in terms of the parameters for the cross section over the resonance, and X', Y' and Z' are new parameters that depend on the same matrix elements presented earlier, as well as

their relative phases. Equation (15) was obtained by the division of two functions of the form of Eq. (11).

The parameters in Eq. (15) have been expressed[37] in terms of the same dipole and Coulomb matrix elements used in the description of the resonance behavior of total and partial cross sections. The expressions derived by Kabachnik and Sazhina describe the resonance effect upon the angular distribution asymmetry parameter, $\beta_t$, for the total photoelectron flux from a given sample. Except possibly for the special case of no interchannel coupling in the continuum, these expressions cannot describe the resonance behavior of the asymmetry parameter, $\beta_\mu$, for an individual photoemission channel in terms of these matrix elements. This is especially true for helium, because as we have seen from the discussion in Sect. III, continuum interactions are important. While the form of Eq. (15) correctly describes these "partial β's", no interpretation of the resulting parameters is yet possible.

## B. Data Analysis

In the present experiment, the resonance behavior of the $He^+(1s)$ and $He^+(n=2)$ partial cross sections and angular distribution asymmetry parameters in the region below the n=3 threshold was measured. The 1s partial cross section is shown in Fig. 6, and the data for the n=2 satellite are shown in Figs. 7 and 9. The sum of the two partial cross sections yields the total cross section (not shown), and their ratio

yields $R_{21}$ shown in Fig. 8. The resonance effects on the 1s partial cross section and the total cross section are proportionately much smaller than those on $\sigma_{n=2}$. The remainder of this section is devoted to a discussion of the fitting techniques and assumptions used to describe analytically the cross-section and asymmetry-parameter data in the resonance region.

The total cross-section data were scaled to the data of Marr and West[1] at the off-resonance energy of 68.9 eV, and the absolute partial cross sections were then scaled from the satellite branching ratio. The total cross-section data, as well as the 1s partial cross-section data, show relatively small changes in the resonance region. For this reason, only the first resonance (3s3p) was discernible from the scatter (2-3%) in the cross-section data, and only this resonance was fitted. The 3s3p resonance was assumed to be isolated for this analysis, because the effect of the next member of the series is less than 1% at the energy of the 3s3p resonance. Both the total cross section and the 1s partial cross section were least-squares fitted to the form of Eq. (5). The position, $E_0$, and width, $\Gamma$, of the resonance were taken from fits by Woodruff and Samson[8] to their data on $\sigma_{n=2}$. For convenience, the monochromator bandpass function was taken to be a Lorentzian with FWHM = 0.17 eV, so that convolution with the resonance width was straightforward. The background intensities for both the total and 1s cross-section data were taken to be linear functions of the photon energy. The Fano parameters from the computer fit to the total cross-section data are listed in Table I.

While the Fano parametrization can be used to interpret the total cross section, it cannot be used to interpret the 1s partial cross section. As discussed in Section IV-A, however, the parameters for the various formalisms can be equated mathematically. Having done so, we report the Starace parameters for photoionization to $He^+(1s)$ over the 3s3p resonance in Table II. The fit to $\sigma_{1s}$ is shown in Fig. 6. Despite the scatter exhibited by our data, we have confidence in the fit because of the good agreement between it and the data of Morin et al.,[10] after accounting for the different photon-energy resolutions used in the two experiments.

The effect of the autoionizing levels on $\sigma_{n=2}$, shown in Fig. 7, is much more pronounced than for either $\sigma_{1s}$ or $\sigma_t$. These data were fitted to the Shore formula, Eq. (10), convoluted with a truncated triangular function of full-width equal to 0.17 eV to account more accurately for monochromator broadening. The off-resonance cross section, C, was taken to be a linear function of energy. The positions and widths of the four resonances were again taken from Woodruff and Samson. The Shore parameters derived in this way are presented in Table III. Note that the values for the fourth resonance were held fixed. The solid curve in Fig. 7 shows this fit, whereas the dashed curve is the same fit, but with the monochromator broadening removed.

The validity of using the Shore parametrization is dependent upon the assumption that the resonances are not coupled in any way, or equivalently, that the series of discrete levels, $\phi_i$, do not perturb each other via Coulomb interactions. Shore[31] has indicated that this

is a good approximation provided that the radiative widths of the resonance states are small compared to their overall widths. Typical radiative lifetimes for allowed dipole transitions are in the range $10^{-8} - 10^{-9}$ sec,[38] so the radiative widths are several orders of magnitude smaller than the resonance widths.

The equivalent Starace parameters for $\sigma_{n=2}$ are also presented in Table III, because they are the most interpretable parameters for a partial cross section. From the approximation in the previous paragraph, we know that the Shore parameters derived from the fit to the $\sigma_{n=2}$ data represent isolated-resonance parameters and can be equated to the Starace parameters. Use of the Shore formula is simply a mathematical construct to derive the appropriate Starace parameters.

The n=2 satellite branching ratio relative to the 1s main line also shows strong resonance effects, as can be seen in Fig. 8, mainly due to the changes in $\sigma_{n=2}$. The branching-ratio data were fitted to a ratio of the two cross sections, $\sigma_{n=2}$ and $\sigma_{1s}$, each written as in Eq. (10). The parameters for the function in the numerator were taken directly from the fit to $\sigma_{n=2}$. For the denominator, $\sigma_{1s}$, the background cross section was taken as a polynomial of second order in energy, and the resonance parameters were varied to get the best fit. The numerator and denominator were convoluted separately with the same monochromator bandpass function used for the fit to the $\sigma_{n=2}$ data. The parameters for $\sigma_{1s}$ for the 3s3p resonance from this fit agree with those derived from the fit to the 1s partial cross-section data alone. The uncertainties in the $\sigma_{1s}$ parameters for the higher-lying resonances

derived from the branching-ratio fit are too large for these parameters to be reported with confidence.

The asymmetry parameter for the n=2 satellite is strongly affected by autoionization, because the peak includes contributions from two satellites with very different off-resonance asymmetry parameters. Our results are shown in Fig. 9. We have also measured $\beta_{1s}$ in the resonance region and found it to be 2.00 ± 0.05, as expected. The $\beta_{n=2}$ data were fitted in a manner identical to the fit to the branching-ratio data, except the parameters in the denominator were taken from the fit to $\sigma_{n=2}$ (Table III). The function used was

$$\beta_{n=2} = \frac{\sum_k \frac{Y_k + X_k\epsilon_k}{1+\epsilon_k^2} + Z}{\sum_k \frac{B_k + A_k\epsilon_k}{1+\epsilon_k^2} + C} \quad . \tag{16}$$

The background value, Z, was assumed to be a second-order polynomial in energy. The resonance parameters, $X_k$ and $Y_k$, are presented in Table IV, where they have been used to determine $X_k'$, $Y_k'$ and $Z_k'$ as in Eq. (15). As with the n=2 partial cross-section fit, we have equated the parameters in the fit to the numerator of $\beta_{n=2}$ with the corresponding single-resonance parameters described by Kabachnik and Sazhina.[37] The parameters $A_k'$, $B_k'$ and $C_k'$ are not shown, but can easily be derived from the values in Table III and Eqs. (15) and (16). We present these "Kabachnik-Sazhina parameters" for $\beta_{n=2}$, with the caveat that the definitions given in Ref. (37) do not allow easy interpretation for an individual photoemission line.

The fit to the $\beta_{n=2}$ data, including monochromator broadening, is shown in Fig. 9. The problem of deconvolution of instrumental broadening from the measured asymmetry parameters is not straightforward, especially when the monochromator bandpass is on the order of, or larger than, the resonance linewidth. The method used here is the same as that described for the fit to $R_{21}$, but using Eq. (16). This method was chosen because the form of Eq. (16) is more amenable to fitting a series of closely-spaced resonances, and because the measured asymmetry parameters are derived from the ratio of peak intensities in two analyzers. The deconvoluted curve is also shown in Fig. 9.

As we have noted above, the derivation by Kabachnik and Sazhina yields parameters that describe the asymmetry parameter, $\beta_t$, for the total photoelectron flux from the helium atom as a function of the photon energy, which is given by

$$\beta_t = \frac{\sigma_{1s}\beta_{1s} + \sigma_{n=2}\beta_{n=2}}{\sigma_{1s} + \sigma_{n=2}} \quad , \tag{17}$$

with $\beta_{1s} = 2$, and $\sigma_{1s}$, $\sigma_{n=2}$ and $\beta_{n=2}$ given by Eqs. (11) and (16) for the 3s3p resonance only. We have restricted this determination of $\beta_t$ to the first resonance, because $\sigma_{1s}$ has not been determined accurately for the others. The resulting $\beta_t$ has the same form as $\beta_{n=2}$, and the Kabachnik-Sazhina parameters describing it are given in Table V. The off-resonance value of $\beta_t$ is approximately 1.8, with deviations due to autoionization of only ~0.1, as expected because the dominant 1s channel shows no effect in $\beta_{1s}$.

## C. Results - Total Cross Section

The results for the total photoionization cross section of helium for the 3s3p resonance are presented in Table I, along with the parameters for the only other measurement[18] of $\sigma_t$ over this resonance. Both Fano and Shore parameters are presented, although the following discussion considers only the Fano parameters. The order-of-magnitude discrepancy in the strength of the resonance, indicated by $\rho^2$, between these two measurements is immediately apparent. Although the only argument we can put forth that the present result is correct is that the total cross-section data are necessarily self-consistent with the data we have measured for $\sigma_{1s}$ and $\sigma_{n=2}$, we can give two reasons why we believe the previous measurement to be inadequate. The first argument is an empirical one. The phase of $\sigma_{1s}$ over the 3s3p resonance that is required by the shape of $\sigma_t$ as measured by Dhez and Ederer[18] combined with the shape of $\sigma_{n=2}$ from the present results (the latter being in agreement with the fluorescence measurements of Woodruff and Samson[8] over the same region) would necessarily have to be opposite of the phase for $\sigma_{n=2}$. This is because the effect on $\sigma_t$ measured by Dhez and Ederer is so small that when the two partial cross sections are added to get the total cross section, their effects have to cancel. This requires that $\sigma_{1s}$ reach a maximum below the resonance energy and a minimum above that energy (compare to $\sigma_{1s}$ in Fig. 6). This conclusion was first reached by Woodruff and Samson,[8] but is inconsistent with our results, as well as other measurements.[10]

Because this cancellation does not occur, the strength of the effect on $\sigma_t$ (as measured by $\rho^2$) must be significantly larger than that measured by Dhez and Ederer. The second argument requires reference to Table I in Ref. (18). This table lists the Shore parameters for a series of five transmission scans taken at three different pressures; 50, 90 and 120 torr. Calculating q and $\rho^2$ for each scan shows a definite pressure dependence of $\rho^2$ (0.009 at 120 torr, 0.013 at 90 torr, and 0.018 at 50 torr). Apparently, this pressure range is too high for the quantitative absorption measurement of this autoionization profile. This may be due to the fact that at these relatively high pressures, most of the photons (>98% at 120 torr) are being absorbed, and an experimental deviation from Beer's Law is occurring. In any case, one of three factors in Eq. (2) of Ref. (18) must be changing with pressure; the path length, $\ell$, the cross section, $\sigma$, or the effective number of atoms, n. An order-of-magnitude change in $\ell$ can be ruled out. The cross section is not likely to be significantly affected at this pressure, because pressure broadening is on the order of a millivolt. Doppler broadening is of the same order and can also be ignored. The value of n, of course, does change with pressure, but it should do so linearly. However, a variation in the exponent of n of only 5% (from 1.0 to 0.95) can account for a factor of 10 in $\rho^2$. Exactly what can cause such a non-linearity for this exponent is unclear, but it seems the most plausible explanation of the pressure dependence of $\rho^2$.

Our value of q also disagrees with the previous result. While this may be due to the same problem as discussed above, it could also

be the result of the normalization procedure used in the earlier work. By normalizing the data at 177.22Å, which is an energy near the center of the resonance, that point is forced to lie on the background curve, fixing the shape of the resonance with respect to the background cross section and thus affecting q.

The present results are also to be compared with previous estimates of the resonance parameters. Fano and Cooper[19] estimated q and $\rho^2$ to be 1.7 and 0.01, respectively. Calculations by Senashenko and Wagué[20] using the diagonalization approximation yielded q = 1.31 and $\rho^2$ = 0.019. Both of these calculations disagree with the values measured here. For the first estimate, however, it may be possible to trace the reasons for this disagreement. In calculating q, Fano and Cooper assumed that the matrix elements involving the $1s\varepsilon p$ continuum state for the 3s3p resonance are not significantly different than similar matrix elements for the 2s2p resonance. This assumption seems to imply, at least, that $\sigma_{1s}$ has the same phase for both the 2s2p and the 3s3p resonances. However, $\sigma_{1s}$ has opposite phases for these two resonances. After consideration of this point, the value of q calculated by Fano and Cooper may be more in line with the present result. For their estimated value of $\rho^2$ = 0.01, part of the discrepancy may be due to the neglect of autoionization into the $He^+(1s)$ continuum. Their estimate from Eq. (6.11) of Ref. (19) is that the effect on $\sigma_{1s}$ should be ~6% for the 3s3p resonance. This effect is similar in absolute magnitude to the effect on $\sigma_{n=2}$. This estimate agrees rather well with our result of an effective $\rho^2$ = 0.046 (Table

II). The low estimate of $\Gamma$ (0.072 eV) may also be improved by inclusion of the 1s contribution. One other calculation[39] of $\sigma_t$ for the 3s3p resonance has also been performed that reproduces the correct qualitative shape of the resonance, but no parameters were extracted because of the small number of points evaluated.

The oscillator strength, $f$, for the 3s3p resonance can be obtained from the Fano parameters for the fit to the total cross section. It is given by[40]

$$f = (0.195\ \mathrm{Ry}^{-1}\mathrm{Mb}^{-1})\ q^2\rho^2\ \sigma_t\Gamma \quad , \tag{18}$$

with $\Gamma$ expressed in Rydbergs and $\sigma_t$ expressed in Mb. Using the values in Table I, we find $f = 2.0 \times 10^{-4}$, which agrees well with the previous estimate[19] of $1.2 \times 10^{-4}$. A similar, but possibly more descriptive, expression for $f$ is obtained[41] by replacing $q^2$ in Eq. (18) with $(q^2 - 1)$. The result for this case is $-8.1 \times 10^{-5}$, indicating that $\sigma_t$ in the vicinity of the 3s3p resonance exhibits a net loss in oscillator strength compared to the background cross section. The latter value of $f$ is more descriptive of autoionization in the sense that it is a measure of the spectral repulsion part of the autoionization profile.

## D. Results - Partial Cross Sections

The results for the $He^+(1s)$ partial cross section for the 3s3p resonance are presented in Table II. Effective Fano parameters are listed in Table II because that formalism was used to fit the $\sigma_{1s}$ data.

The Starace parameters are the most descriptive representation of the data. They can be used, along with similar values for $\sigma_{n=2}$, to derive $\alpha_\mu$-parameters and, ultimately, matrix elements describing the autoionization process.

This work represents the first measurement of these parameters for the 3s3p resonance. Again, we note that the $\sigma_{1s}$ profile has the same phase as $\sigma_t$ and as $\sigma_{n=2}$ (see Figs. 6 and 7). The parameters for $\sigma_{n=2}$ for the first four members of the Rydberg series leading to the n=3 threshold are listed in Table III, along with the results of Woodruff and Samson.[8] The Shore parameters were found by fitting the data to Eq. (10) as described in Section IV-B, and the Starace parameters were then derived. The parameters for each member of the Rydberg series are fairly similar, as originally predicted by Fano and Cooper.[19] The energy and width of each resonance were taken from the work of Woodruff and Samson.[8] Results of several calculations[20,29,39,42-46] of these positions and widths are summarized in Ref. (8). Differences in the background cross sections (C and $\sigma_0$ in Table III) are due to differences in the scaling of the present data and the data in Ref. (8).

Although, as we have pointed out, it is generally impossible to determine all three unknowns in Eq. (14), the simplicity of the helium system allows us to do so in a manner similar to the method described in an earlier paper.[36] The following discussion is limited to the 3s3p resonance, but similar results are expected for the higher-lying resonances. For $He^+(1s)$ production, there are only two outgoing channels, $\mu$: $1s\varepsilon p_{1/2}$ and $1s\varepsilon p_{3/2}$. The dipole and Coulomb matrix

elements for these two channels help determine two of the $\alpha_\mu$-parameters: $\alpha_{1s\epsilon p_{1/2}}$ and $\alpha_{1s\epsilon p_{3/2}}$. Of course, both of these channels are present in the $He^+(1s)$ peak (m=1s). In this case, however, because the spin-orbit interaction in the $\epsilon p$ continuum is small, and because $\beta_{1s}$ is identically 2.0 over the resonance, the Schwartz inequality, Eq. (14), becomes an equality. Equations (11), (12) and (14) and the Starace parameters in Table II may then be used to obtain $Re\langle\alpha\rangle_{1s}$, $Im\langle\alpha\rangle_{1s}$ and $\langle|\alpha|^2\rangle_{1s}$. The solution involves a complicated quadratic equation for $Re\langle\alpha\rangle_{1s}$. The solution with $\langle|\alpha|^2\rangle_{1s} > 2$ is dismissed, because it would require that the total cross section have $\rho^2 > 1$. The parameters for the correct solution are given in Table VI. It is also possible to determine the non-averaged quantities, $Re(\alpha_{1s\epsilon p_j})$, $Im(\alpha_{1s\epsilon p_j})$ and $|\alpha_{1s\epsilon p_j}|^2$, where j can have the values 1/2 or 3/2, because our earlier assumption that Eq. (14) is an equality means that the matrix elements for the two outgoing channels in the 1s peak are identical for the dipole and Coulomb interactions. The averaged quantities for the $1s\epsilon p$ final state in Table VI are then just averages of identical quantities. The resulting non-averaged $\alpha$-parameters are not listed because their values are identical to the averaged quantities listed in Table VI.

From Eqs. (15) and (16) in Ref. (36), we can determine the partial linewidths, $\Gamma_{1s}$ and $\Gamma_{n=2}$, for the two final states. Both of these partial widths are included in Table VI. The large difference in the partial widths illustrates why the effect of the resonance on $\sigma_{1s}$ is small relative to the effect on $\sigma_{n=2}$, even though $\sigma_0(1s)$ is an order of magnitude larger than $\sigma_0(n=2)$. The partial widths can be interpreted

as an additional measure ($\langle |\alpha|^2 \rangle_m$ is the other one) of the strength of the resonance effect on an individual final state. As we did with the $\alpha$-parameters for the 1s level, we can break down the contributions to $\Gamma_{1s}$ into partial widths for each outgoing channel, being careful to account for the multiplicities of the two outgoing channels. The results are $\Gamma_{1s\varepsilon p_{1/2}}/\Gamma = 0.004$ and $\Gamma_{1s\varepsilon p_{3/2}}/\Gamma = 0.009$. The partial widths (in percent) derived here agree very well with previous calculations.[20,29]

Because we have already found $\langle |\alpha|^2 \rangle_{1s}$, we can use Eq. (17) in Ref. (35) to find $\langle |\alpha|^2 \rangle_{n=2}$. Having done this, $C_1(n=2)$ and $C_2(n=2)$ for the 3s3p resonance from Table III can be used with Eqs. (11) and (12) to find $\mathrm{Re}\langle \alpha \rangle_{n=2}$ and $\mathrm{Im}\langle \alpha \rangle_{n=2}$. These values are also presented in Table VI. We note that for the $\alpha$-parameters for $\sigma_{n=2}$, Eq. (14) appears to be a true inequality. Because the satellite peak containing the 2s and 2p final states includes seven possible outgoing channels, no further information can be obtained.

A check of the $\alpha_\mu$-parameters can be made as described in Ref. (36). The results in Table VI satisfy this check to well within the statistical errors, suggesting that no major systematic errors are present in the data analysis.

Some interpretation of the $\alpha_\mu$-parameters can be made. The positive values of $\mathrm{Re}\langle \alpha \rangle_m$ for both the 1s and n=2 levels indicate that these two resonance profiles should have the same phase over the resonance, as we have observed. The approximately zero values for $\mathrm{Im}\langle \alpha \rangle_{1s}$ and $\mathrm{Im}\langle \alpha \rangle_{n=2}$ show that the $\alpha_\mu$-parameters are essentially real

numbers. This result seems fortuitous, because it probably does not imply, as discussed by Combet Farnoux,[34] that interchannel coupling in the continuum is weak. In fact, because the n=2 peak is a satellite of the 1s peak, interchannel coupling in this case is important (see Sect. III). It might prove interesting to measure the $\alpha$-parameters for the individual final states, 2s and 2p. The strong coupling between $2s\varepsilon p$ and $2p\varepsilon s$ may result in $\alpha$-parameters that are complex. A detailed flourescence experiment, similar to that done by Woodruff and Samson,[8] could measure these parameters.

To this point, we have only derived parameters which depend on several of the dipole and Coulomb matrix elements. It is possible, however, for the case of the 3s3p resonance, to determine directly the squares of three of the matrix elements, including all of those describing autoionization into the $1s\varepsilon p$ continuum. The Coulomb matrix elements $|\langle 3s3p|V|1s\varepsilon p_j\rangle|^2$, with j=1/2 or 3/2, can be obtained from Eq. (8) for the partial decay width, $\Gamma_{1s} = 0.0023$ eV, by properly accounting for the multiplicity of the $1s\varepsilon p_j$ states. The dipole matrix elements for continuum absorption, $|\langle 1s\varepsilon p_j|\vec{r}|1s^2\rangle|^2$, can be determined from $\sigma_{1s}$ as described in Ref. (19) and again considering the multiplicities. The dipole matrix elements can also be expressed as oscillator strengths. The dipole matrix element for the discrete transition $1s^2 \rightarrow 3s3p$ can be determined[19] from the oscillator strength, $f$, derived in Section IV-C. All of these results are listed in Table VII, along with estimates of two of the matrix elements by Fano and Cooper.[19] Their results agree with ours to within a factor of 2.

One additional parameter can also be derived. The square of the term in brackets in Eq. (14) can be determined by using $\langle |\alpha|^2 \rangle_{1s}$ from Table VI and the matrix elements in Table VII. We find this term to have the value 36 $Mb/Ry^2$.

## E. Results - Asymmetry Parameters

The data in Fig. 9 mark the first detailed measurement of a satellite asymmetry parameter over autoionization resonances. The accompanying parameters in Table IV vary only slightly over the members of the Rydberg series, as first predicted by Dill.[47]

Because the angular distributions of all of the helium photoemission peaks (there are only 2) were measured in this experiment, it is possible to derive parameters from the $\beta_t$ data that have been expressed in terms of the appropriate dipole and Coulomb matrix elements. The formalism and data analysis method were discussed in earlier sections, and the results are listed in Table V. It is hoped that these results, as well as those for $\beta_{n=2}$, will spur further theoretical development regarding the detailed behavior of angular distributions of individual photoemission lines in the vicinity of autoionization resonances. Complete understanding of this phenomenon awaits further theoretical and experimental work.

In Section III we were able to derive the ratio $R=\sigma_{2p}/\sigma_{2s}$ from the measured off-resonance $\beta_{n=2}$ data and calculated values of $\beta_{2p}$. We are unable to do this in the resonance region because the resonance behavior

of $\beta_{2p}$ is unknown, but certain qualitative statements can be made concerning the effects on R of the 3s3p resonance. For the following discussion, the reader is referred to the deconvoluted curves in Figs. 7 and 9.

Figure 7 shows that the n=2 partial cross section drops nearly to zero at the minimum of the 3s3p resonance. From Fig. 5, the background value of R at 70 eV is ~2.2. To account for the minimum in $\sigma_{n=2}$, both $\sigma_{2p}$ and $\sigma_{2s}$ must be going through a minimum at the energy of the minimum in $\sigma_{n=2}$. Furthermore, both of these minima occur on the low-energy side of the 3s3p resonance. In other words, we can conclude that both $\sigma_{2p}$ and $\sigma_{2s}$ are affected by the resonance and that they have the same phase. The question then arises of whether or not these effects manifest themselves in an effect on R. If R is left unaffected, then the measured change in $\beta_{n=2}$ (see Eq. (3)) must be due solely to changes in $\beta_{2p}$ (assuming that $\beta_{2s}$ is always 2.0, just like $\beta_{1s}$). However, examination of the minimum in $\beta_{n=2}$ on the high-energy side of the resonance shows that even if $\beta_{2p} = -1$ at this energy, a value of $R = 2.2$ is not large enough to yield (see Eq. (4)) the deconvoluted value of $\beta_{n=2} = -0.25$ from Fig. 9. The values of $R = 2.2$ and $\beta_{2p} = -1$ yield $\beta_{n=2} = -0.06$. The uncertainty in the minimum of the deconvoluted curve for $\beta_{n=2}$ is ~0.1. Therefore, our value of $\beta_{n=2} = -0.25$ suggests that R shows a positive deviation from its background value of 2.2 on the high-energy side of the 3s3p resonance. Because R must have the same shape as the satellite branching-ratio over an autoionization resonance, it must reach a minimum on the low-energy side of the 3s3p

resonance as well. No limits can be placed on the value of this minimum. The conclusion then, is that R drops to a minimum on the low-energy side and rises to a maximum on the high-energy side of the 3s3p resonance. This behavior is most likely caused by $\sigma_{2p}$ and $\sigma_{2s}$ having similar profiles, but with $\sigma_{2p}$ reaching its minimum at a slightly lower energy than $\sigma_{2s}$. This implies that the Starace parameters, $C_1(2p)$ and $C_2(2p)$ are slightly larger than $C_1(2s)$ and $C_2(2s)$, respectively. We expect the higher members of this series to have similar effects on R, because partial cross sections tend to retain the same shape over a Rydberg series.[19]

## V. Conclusion

The photoionization of helium to the n=2 excited state of the helium ion has provided several interesting results. The off-resonance measurements of $\beta_{n=2}$ have shown additional clear evidence that the n=2 satellite is mainly comprised of the 2p final state near threshold. Furthermore, the strong energy dependence of R has given some insight into the understanding of electron correlation in atomic systems: the helium case being especially useful because of its relative simplicity.

A new measurement of the total cross section over the 3s3p resonance has been performed. The correlation coefficient, $\rho^2$, is an order of magnitude larger than in the previous study, but the new value has been shown to be consistent with measurements of $\sigma_{1s}$ over this resonance. The new Fano q parameter also differs from the previous result. More work at higher resolution on the the total cross section of helium above the $n\geq 2$ thresholds is recommended to verify our conclusions.

We have presented the first detailed measurement of $\sigma_{1s}$ for the 3s3p resonance, allowing us to extract parameters describing the autoionization process to the $1s\varepsilon p$ continuum. In particular, we were able to derive the squares of individual matrix elements governing the interactions of the discrete autoionizing state with the ground and continuum levels.

For the $He^+(n=2)$ satellite, the partial cross-section and asymmetry-parameter behavior has been measured over the major Rydberg

series leading to the n=3 threshold. These angular-distribution measurements are the first of their kind for a satellite line. Parameters describing all of these resonance effects have been presented. From the angular-distribution results, the qualitative behavior of R over the resonances has been inferred.

Acknowledgements

The authors would like to thank J.A. Richards and F.P. Larkins and the Orsay group (Ref. 10) for providing their results prior to publication. We would also like to thank J.A. Richards, F.P. Larkins and F. Wuilleumier for helpful discussions.

This work was supported by the Director, Office of Energy Research, Office of Basic Energy Sciences, Chemical Sciences Division of the U.S. Department of Energy under Contract No. DE-AC03-76SF00098. It was performed at the Stanford Synchrotron Radiation Laboratory, which is supported by the NSF through the Division of Materials Research. One of us (U.B.) would like to acknowledge support by the Deutsche Forschungsgemeinschaft and another (H.G.K.) by a Wigner fellowship.

References

1. G.V. Marr and J.B. West, At. Data and Nuc. Data Tables 18, 497 (1976).
2. G. Wendin, J. Phys. B 4, 1080 (1971): T. Ishihara and R.T. Poe, Phys. Rev. A 6, 116 (1972): M.Y. Amusia, N.A. Cherepkov, D. Živanović and V. Radojević, Phys. Rev. A 13, 1466 (1976).
3. J.A.R. Samson, Phys. Rev. Lett. 22, 693 (1969).
4. M.O. Krause and F. Wuilleumier, J. Phys. B 5, L143 (1972).
5. P.R. Woodruff and J.A.R. Samson, Phys. Rev. Lett. 45, 110 (1980).
6. F. Wuilleumier, M.Y. Adam, N. Sandner and V. Schmidt, J. Physique-Lett. 41, L373 (1980).
7. J.M. Bizau, F. Wuilleumier, P Dhez, D.L. Ederer, T.N. Chang, S. Krummacher and V. Schmidt, Phys. Rev. Lett. 48, 588 (1982).
8. P.R. Woodruff and J.A.R. Samson, Phys. Rev. A 25, 848 (1982).
9. V. Schmidt, H. Derenbach and R. Malutzki, J. Phys. B 15, L523 (1982).
10. P. Morin, M.Y. Adam, I. Nenner, J. Delwiche, M.J. Hubin-Franskin and P. Lablanquie, to be published.
11. E.E. Salpeter and M.H. Zaidi, Phys. Rev. 125, 248 (1962).
12. V. Jacobs, Phys. Rev. A 3, 289 (1971).
13. V.L. Jacobs and P.G. Burke, J. Phys. B 5, L67 (1972).
14. T.N. Chang, J. Phys. B 13, L551 (1980).
15. J.A. Richards, Honours Thesis, Monash Univ., Australia (1981).
16. K.A. Berrington, P.G. Burke, W.C. Fon and K.T. Taylor, J. Phys. B 15, L603 (1982).

17. F.P. Larkins, International Conference on X-ray and Atomic Inner-shell Physics (X-82), AIP Conference Proc. No. 94, Ed. B. Crasemann, American Institute of Physics, New York (1982).

18. P. Dhez and D.L. Ederer, J. Phys. B 6, L59 (1973).

19. U. Fano and J.W. Cooper, Phys. Rev. 137, A1364 (1965).

20. V.S. Senashenko and A. Wagué, J. Phys. B 12, L269 (1979).

21. S.H. Southworth, C.M. Truesdale, P.H. Kobrin, D.W. Lindle, W.D. Brewer and D.A. Shirley, J. Chem. Phys. 76, 143 (1982).

22. M.G. White, R.A. Rosenberg, G. Gabor, E.D. Poliakoff, G. Thornton, S.H. Southworth and D.A. Shirley, Rev. Sci. Instr. 50, 1268 (1979).

23. J.A. Richards and F.P. Larkins, private communication.

24. T. Ishihara, J. Mizuno and T. Watanabe, Phys. Rev. A, 22, 1552 (1980).

25. H.P. Kelly, Phys. Rev. A 6, 1048 (1972).

26. R.L. Brown, Phys. Rev. A 1, 341 (1970).

27. J.M. Bizau, F.J. Wuilleumier, D.L. Ederer, P. Dhez, S. Krummacher and V. Schmidt, to be published.

28. R.P. Madden and K. Codling, Astrophys. J. 141, 364 (1965).

29. D.R. Herrick and O. Sinanoğlu, Phys. Rev. A 11, 97 (1975).

30. U. Fano, Phys. Rev. 124, 1866 (1961).

31. B.W. Shore, Phys. Rev. 171, 43 (1968).

32. A.F. Starace, Phys. Rev. A 16, 231 (1977).

33. L.C. Davis and L.A. Feldkamp, Phys. Rev. B 23, 6239 (1981).

34. F. Combet Farnoux, Phys. Rev. A 25, 287 (1982).

35. P.C. Kemeny, J.A.R. Samson and A.F. Starace, J. Phys. B 10, L201 (1977).

36. P.H. Kobrin, U. Becker, S. Southworth, C.M. Truesdale, D.W. Lindle and D.A. Shirley, Phys. Rev. A 26, 842 (1982).

37. N.M. Kabachnik and I.P. Sazhina, J. Phys. B 9, 1681 (1976).

38. G. Herzberg, Molecular Spectra and Molecular Structure I. Spectra of Diatomic Molecules (Van Nostrand, New York, 1950).

39. S. Ormonde, W. Whitaker and L. Lipsky, Phys. Rev. Lett. 19, 1161 (1967).

40. U. Fano and J.W. Cooper, Rev. Mod. Phys. 40, 441 (1968).

41. P.G. Burke and D.D. McVicar, Proc. Phys. Soc. (London) 86, 989 (1965).

42. P.G. Burke and A.J. Taylor, J. Phys. B 2, 44 (1969).

43. R.S. Oberoi, J. Phys. B 5, 1120 (1972).

44. K.T. Chung and I. Chen, Phys. Rev. Lett. 28, 783 (1972).

45. Y.K. Ho, J. Phys. B 12, 387 (1979).

46. Y.K. Ho, J. Phys. B 15, L691 (1982).

47. D. Dill, Phys. Rev. A 7, 1976 (1973).

Table I. Parameters for the total cross section of helium for the 3s3p resonance. The background cross section, $\sigma_0$ (Mb), was taken to be 3.08 - 0.0300(E), where E is the photon energy in eV. The numbers in parentheses represent statistical errors only.

| | Fano parameters | | | Shore parameters(Mb) | |
|---|---|---|---|---|---|
| | This work | DE[a] | | This work | DE[a] |
| q | 0.84(30) | 1.36(20) | A | 0.18(8) | 0.032(6) |
| $\rho^2$ | 0.11(3) | 0.012(3) | B | -0.032(56) | 0.010(5) |
| $\sigma_0$(Mb) | 0.989(20) | 0.957(30) | C | 0.989(20) | 0.957(30) |
| $\Gamma$(eV) | 0.178(12)[b] | 0.132(14) | | | |
| $E_0$(eV) | 69.917(12)[b] | 69.919(7) | | | |

[a]Dhez and Ederer, Ref. (18).

[b]From Ref. (8). Same for all fits in this work.

Table II. Parameters for the $He^+(1s)$ partial cross section for the 3s3p resonance. The background cross section, $\sigma_0$ (Mb), was taken to be 2.87 - 0.0283(E), where E is the photon energy in eV. Numbers in parentheses represent statistical errors only.

| Effective Fano parameters[a] | Starace parameters[a] |
|---|---|
| $q = 1.1(3)$ | $C_1 = 1.01(3)$ |
| $\rho^2 = 0.046(30)$ | $C_2 = 0.10(7)$ |
| $\sigma_0 = 0.892(20)$ Mb | $\sigma_0 = 0.892(20)$ Mb |

[a] $E_0 = 69.917(12)$ eV and $\Gamma = 0.178(12)$ eV from Ref. (8).

Table III. Parameters for the $He^+(n=2)$ partial cross section for the first 4 members of the $1_n$ Rydberg series. The background cross section, $\sigma_0$ (Mb), was taken to be 0.216 - 0.0017(E), where E is the photon energy in eV. Numbers in parentheses represent statistical errors only.

| | | Shore parameters(Mb) | | | Starace parameters | |
|---|---|---|---|---|---|---|
| Resonance | | This work | WS[a] | | This work | WS[a] |
| $1_3$ | A | 0.120(2) | 0.081(14) | $C_1$ | 0.55(2) | 0.24(11) |
| $E_0$=69.917 eV[a] | B | -0.044(2) | -0.065(8) | $C_2$ | 1.24(2) | 0.94(18) |
| $\Gamma$=0.178 eV[a] | C | 0.097(1) | 0.086(7) | $\sigma_0$(Mb) | 0.097(1) | 0.086(7) |
| $1_4$ | A | 0.086(5) | 0.079(17) | $C_1$ | 0.35(5) | 0.23(13) |
| $E_0$=71.601 eV[a] | B | -0.061(5) | -0.066(10) | $C_2$ | 0.92(5) | 0.92(21) |
| $\Gamma$=0.096 eV[a] | C | 0.094(1) | 0.086(7) | $\sigma_0$(Mb) | 0.094(1) | 0.086(7) |
| $1_5$ | A | 0.080(7) | 0.088(21) | $C_1$ | 0.45(8) | 0.49(15) |
| $E_0$=72.181 eV[a] | B | -0.051(7) | -0.044(12) | $C_2$ | 0.86(8) | 1.02(26) |
| $\Gamma$=0.067 eV[a] | C | 0.093(1) | 0.086(7) | $\sigma_0$(Mb) | 0.093(1) | 0.086(7) |
| $1_6$ | A | 0.080(fix) | 0.085(28) | $C_1$ | 0.45(fix) | 0.23(20) |
| $E_0$=72.453 eV[a] | B | -0.051(fix) | -0.066(16) | $C_2$ | 0.86(fix) | 0.99(34) |
| $\Gamma$=0.038 eV[a] | C | 0.093(1) | 0.086(7) | $\sigma_0$(Mb) | 0.093(1) | 0.086(7) |

[a]Woodruff and Samson, Ref. (8).

Table IV. Parameters for $\beta_{n=2}$ for the first 4 members of the $1_n$ Rydberg series. The background value, Z (Mb), was taken to be $2.28 + 0.0103(E) - 0.00061(E^2)$, where E is the photon energy in eV. Numbers in parentheses represent statistical errors only.

| | Fit parameters(Mb) | | | KS parameters(Mb)[a] | | |
|---|---|---|---|---|---|---|
| Resonance | X | Y | Z | X' | Y' | Z' |
| $1_3$ | -0.030(6) | -0.037(5) | 0.021(1) | 0.021(1) | -0.030(6) | -0.016(5) |
| $1_4$ | -0.031(9) | -0.037(9) | 0.036(2) | 0.036(2) | -0.031(9) | -0.001(9) |
| $1_5$ | -0.031(14) | -0.040(14) | 0.041(3) | 0.041(3) | -0.031(14) | 0.001(14) |
| $1_6$ | -0.031(fix) | -0.040(fix) | 0.043(3) | 0.043(3) | -0.031(fix) | 0.003(fix) |

[a]Kabachnik and Sazhina, Ref. (37).

Table V. Kabachnik-Sazhina parameters for the angular distribution of the total photoelectron flux from helium for the 3s3p resonance. The numbers in parentheses represent statistical errors only.

| | |
|---|---|
| X' = 1.81(4) | A' = 0.99(2) |
| Y' = 0.15(13) | B' = 0.18(8) |
| Z' = 1.79(7) | C' = 0.96(6) |

Table VI. $\alpha$-parameters and partial linewidths for the 3s3p resonance.

| Final state | $Re\langle\alpha\rangle_m$ | $Im\langle\alpha\rangle_m$ | $\lvert\langle\alpha\rangle^2\rvert_m$ | $(\Gamma_m/\Gamma)\times 100$ |
|---|---|---|---|---|
| $1s\epsilon p$ | 0.023(21) | −0.03(4) | $0.0016\ ^{+0.0020}_{-0.0016}$ | $1.3\ ^{+1.7}_{-1.3}$ |
| $2s\epsilon p$, $2p\epsilon s$ } n=2 | 0.99(15) | 0.2(3) | 1.1(3) | $98.7\ ^{+1.3}_{-1.7}$ |

Table VII. Matrix elements for the 3s3p resonance.

| Matrix element | Amplitude: This work | Amplitude: Fano and Cooper[19] |
|---|---|---|
| $\lvert\langle 3s3p\lvert\vec{r}\rvert 1s^2\rangle\rvert^2$ | $1.1 \times 10^{-3}$ Mb | $6.8 \times 10^{-4}$ Mb |
| $\lvert\langle 1s\varepsilon p_j\lvert\vec{r}\rvert 1s^2\rangle\rvert^{2}$ [a,b] | 0.10 Mb/Ry | |
| $\lvert\langle 3s3p\lvert V\rvert 1s\varepsilon p_j\rangle\rvert^{2}$ [b] | $4.5 \times 10^{-6}$ Ry | $4.7 \times 10^{-6}$ Ry[c] |

[a] The corresponding oscillator strength, $df/dE$, is 0.0014 $eV^{-1}$.

[b] $j = 1/2, 3/2$.

[c] The value given by Fano and Cooper is for the sum over all the channels contributing to the 1s peak. We have divided their value by 6 for comparison.

Figure Captions

Fig. 1 Energy-level diagram for helium. DI = direct ionization. AI = autoionization. The energy scale above the break is expanded four times relative to the energy scale below the break.

Fig. 2 TOF photoelectron spectrum of helium taken at a photon energy of 80 eV at $\theta = 0^{\circ}$, converted to a kinetic-energy scale.

Fig. 3 Branching ratio, $R_{21} = \sigma_{n=2}/\sigma_{1s}$, for the $He^{+}(n=2)$ satellite relative to the 1s main line. Experimental results; ● - present results; ■ - Samson, Ref. 3; ○ - Krause and Wuilleumier, Ref. 4; X - Wuilleumier et al., Ref. 6. Theoretical curves;—– - Salpeter and Zaidi, Ref. 11;——· Jacobs, Ref. 12; —— Jacobs and Burke, Ref. 13;———Chang, Ref. 14;– – – Richards, Ref. 15. Where applicable, we have plotted only the velocity results for consistency.[12-15]

Fig. 4 Asymmetry parameter of the $He^{+}(n=2)$ satellite as a function of photon energy. Experimental results; ● - present results; ○ - Bizau et al., Ref. 7; X - Schmidt et al., Ref. 9; □ - Morin et al., Ref. 10. Some error bars have been omitted for clarity. Theoretical curves; —— Jacobs and Burke, Ref. 13;——— Chang from Bizau et al., Ref. 7. Also shown are calculations of the asymmetry parameter for the 2p final state by Jacobs and Burke[13] and Chang.[7] The velocity forms of the calculations have been plotted in all cases.

Fig. 5 The subshell branching ratio, $R = \sigma_{2p}/\sigma_{2s}$, for the $He^+(n=2)$ satellite as a function of photon energy. Experimental results; ● - present results; ■ - Woodruff and Samson, Ref. 8; ○ - Bizau et al., Ref. 7; X - Schmidt et al., Ref. 9; □ - Morin et al., Ref. 10. Some error bars have been omitted for clarity. Theoretical curves;——· Jacobs, Ref. 12;——Jacobs and Burke, Ref. 13;— —Chang, Ref. 14;- - - Richards and Larkins, Ref. 17;—— Berrington et al., Ref. 16. From Berrington et al. we show the length form of their calculation, which the authors predict to be more accurate than the velocity form. The remainder of the curves are velocity forms.

Fig. 6 Partial cross section of the $He^+(1s)$ main line in the vicinity of the 3s3p resonance, scaled to the data of Marr and West[1] at $h\nu = 68.9$ eV. The solid curve is a fit to the data using Eq. (5a). The dashed curve represents the data of Morin et al. (Ref. 10) taken with a monochromator bandpass of 0.44 eV. The data of Ref. 10 show scatter of 3-4% about this curve. We have shifted their data along both axes for ease of comparison.

Fig. 7 Partial cross section of the $He^+(n=2)$ satellite in the resonance region below the n=3 threshold, scaled as for the $\sigma_{1s}$ data in Fig. 6. The solid curve is a fit to the data using the form of Eq. (10). The dashed curve is the same fit with the monochromator broadening of 0.17 eV removed.

Fig. 8 Branching ratio, $R_{21} = \sigma_{n=2}/\sigma_{1s}$, for the $He^+(n=2)$ satellite relative to the 1s main line in the resonance region below the n=3 threshold. The solid and dashed curves are fits to the data with and without monochromator broadening, respectively, as described in the text.

Fig. 9 Asymmetry parameter of the $He^+(n=2)$ satellite in the resonance region below the n=3 threshold. The solid curve is a fit to the data using the form of Eq. (16). The dashed curve is the same fit with the monochromator broadening removed by the method described in the text.

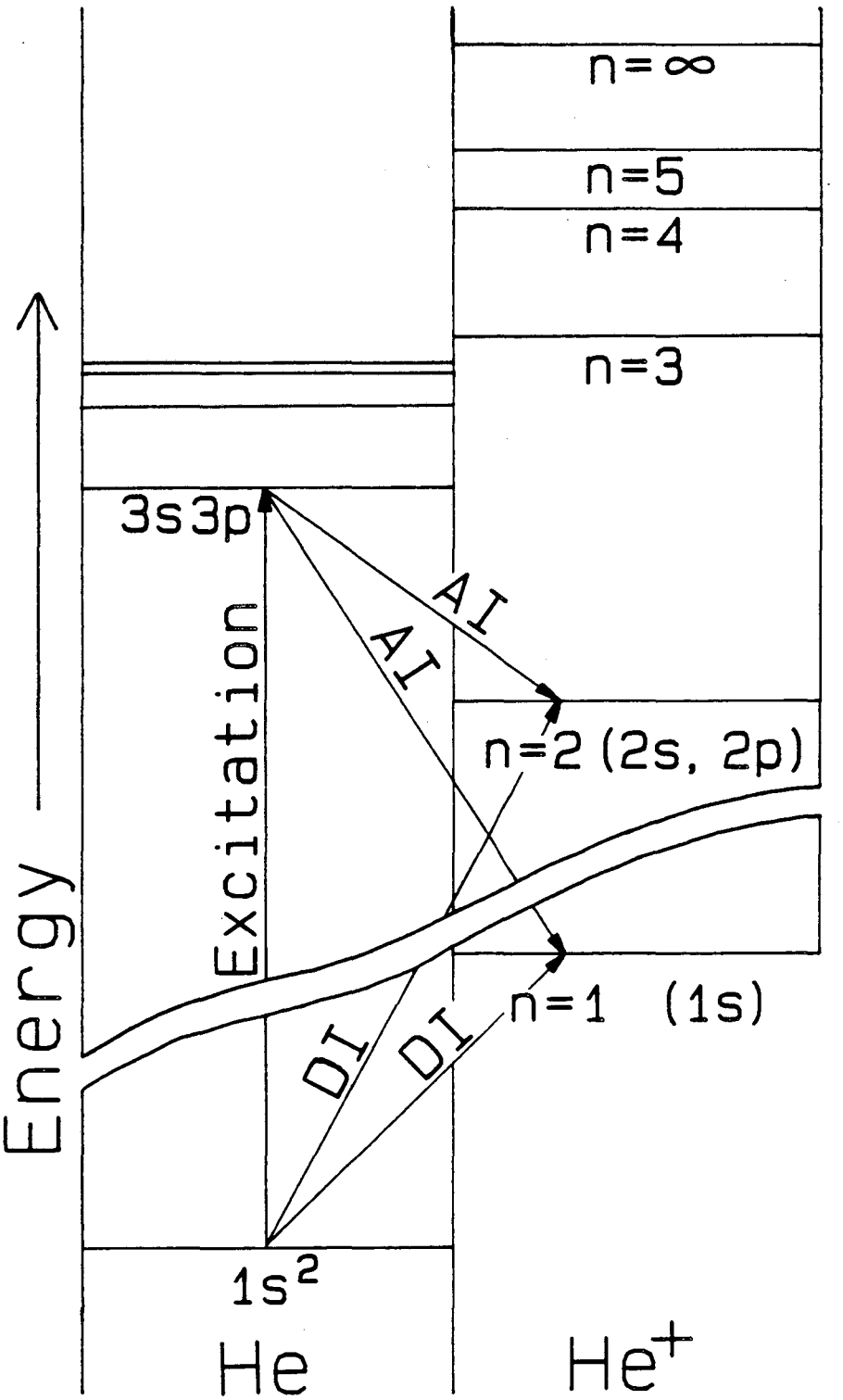


XBL 834-9460

Figure 1

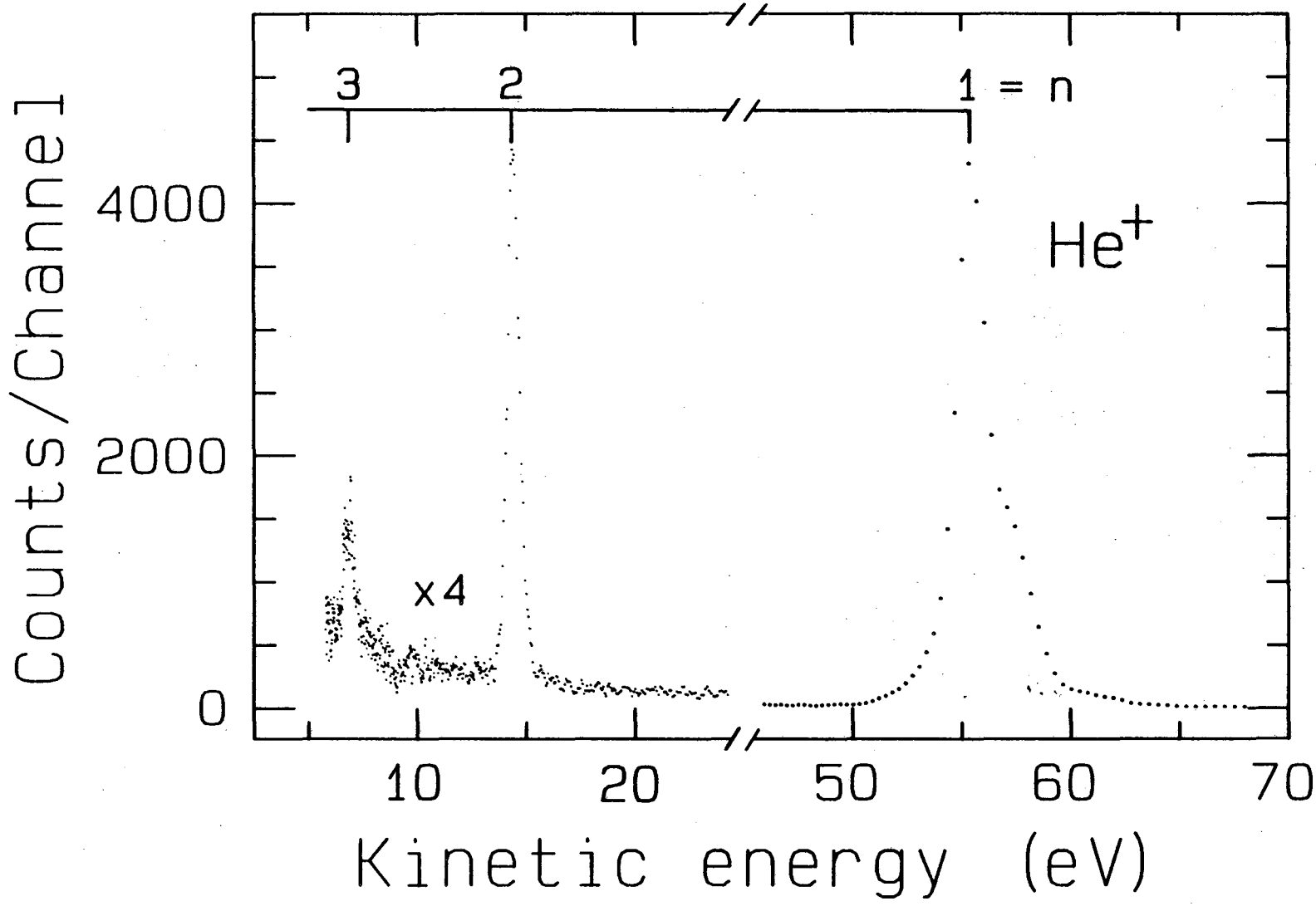


XBL 834-9461

Figure 2

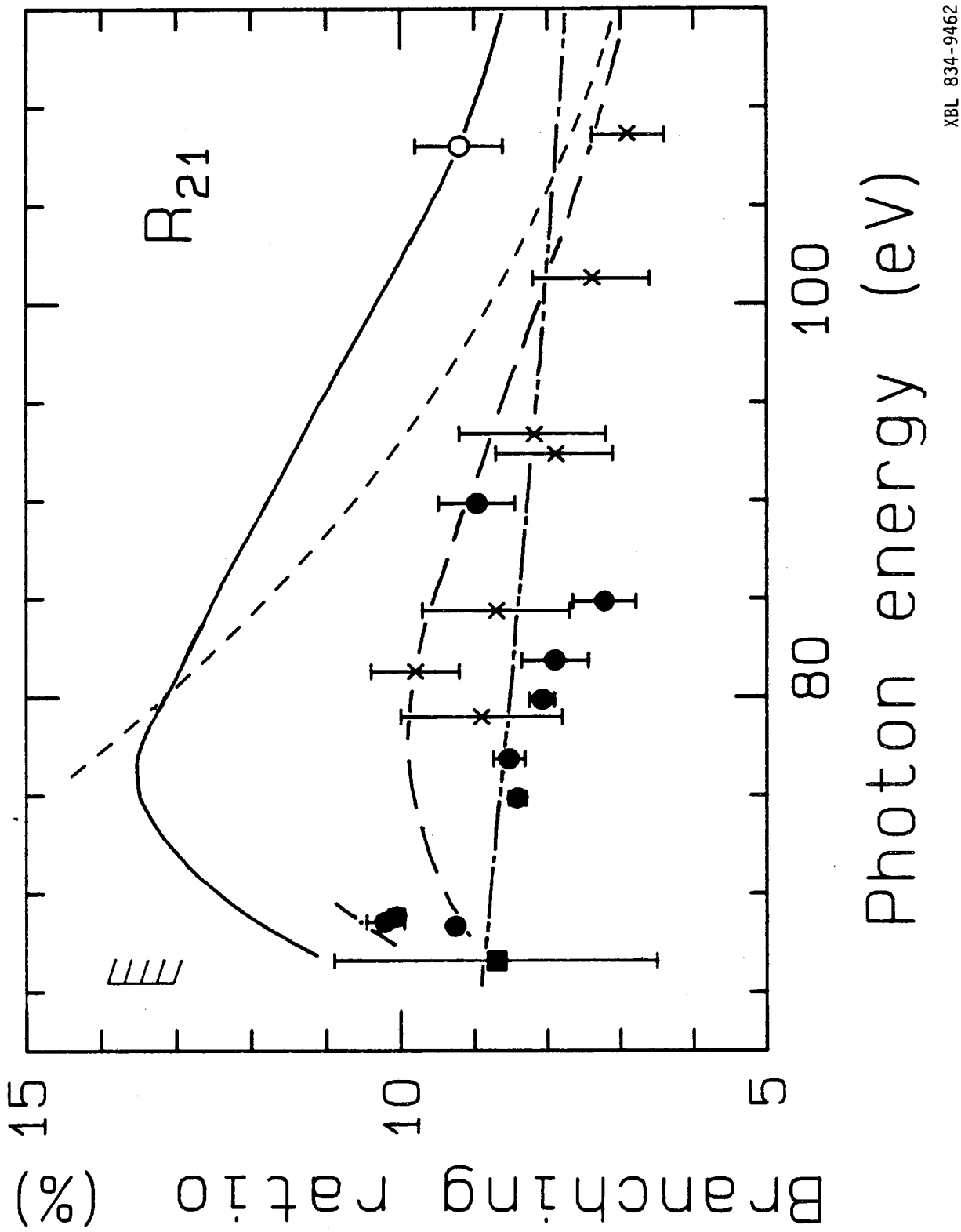


XBL 834-9462

Figure 3

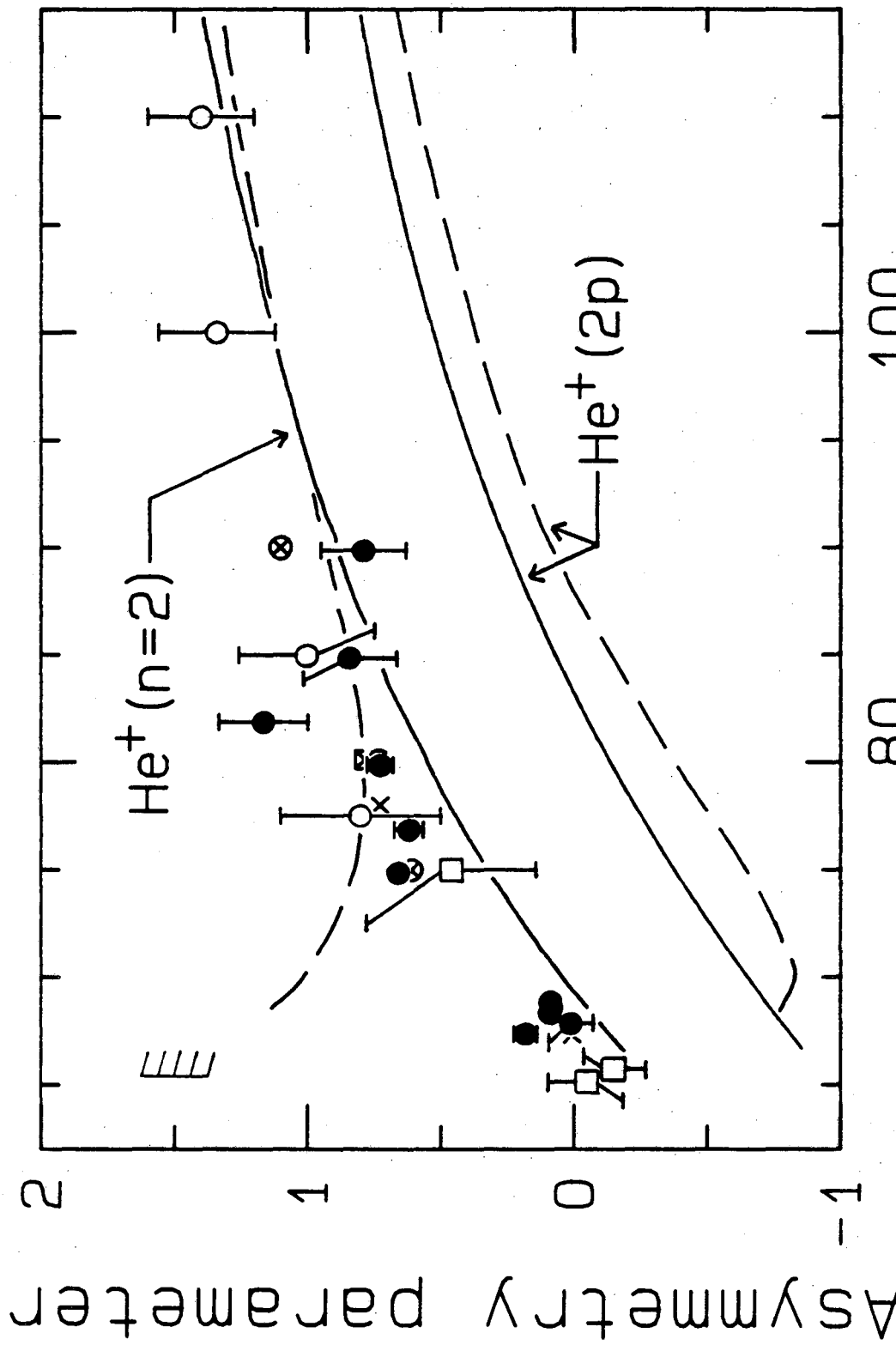


XBL 834-9463

Figure 4

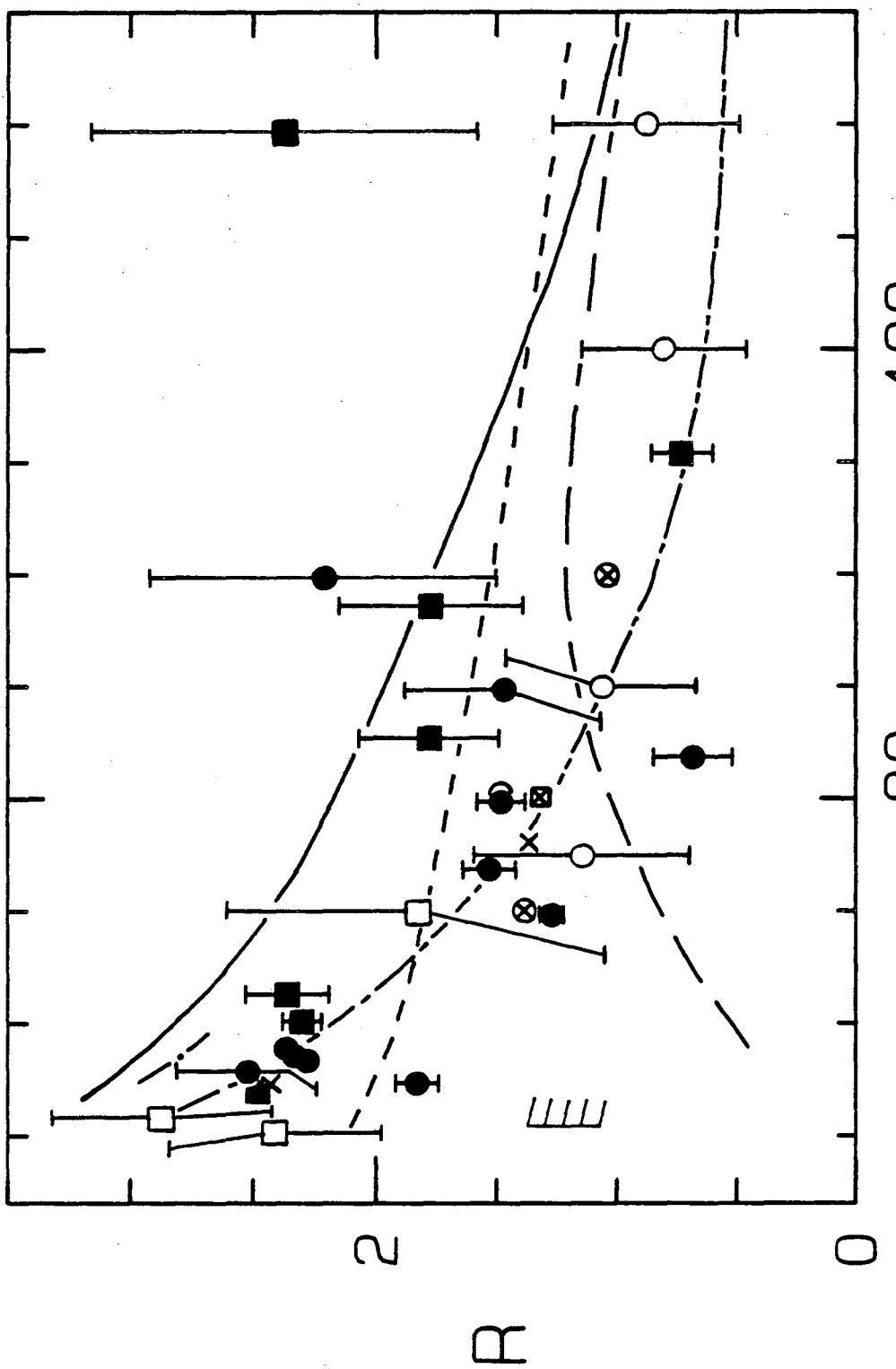


XBL 834-9464

Figure 5

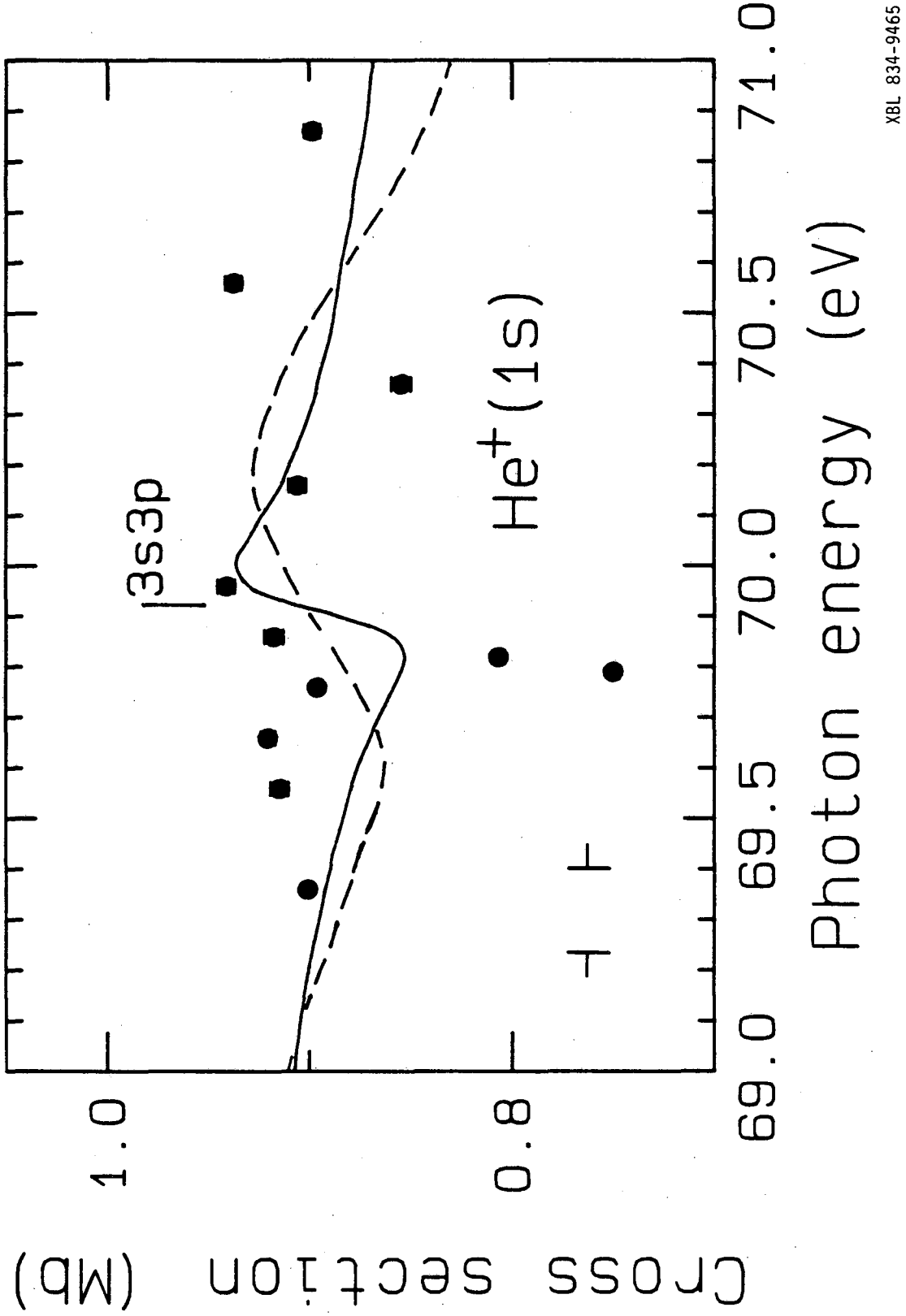


XBL 834-9465

Figure 6

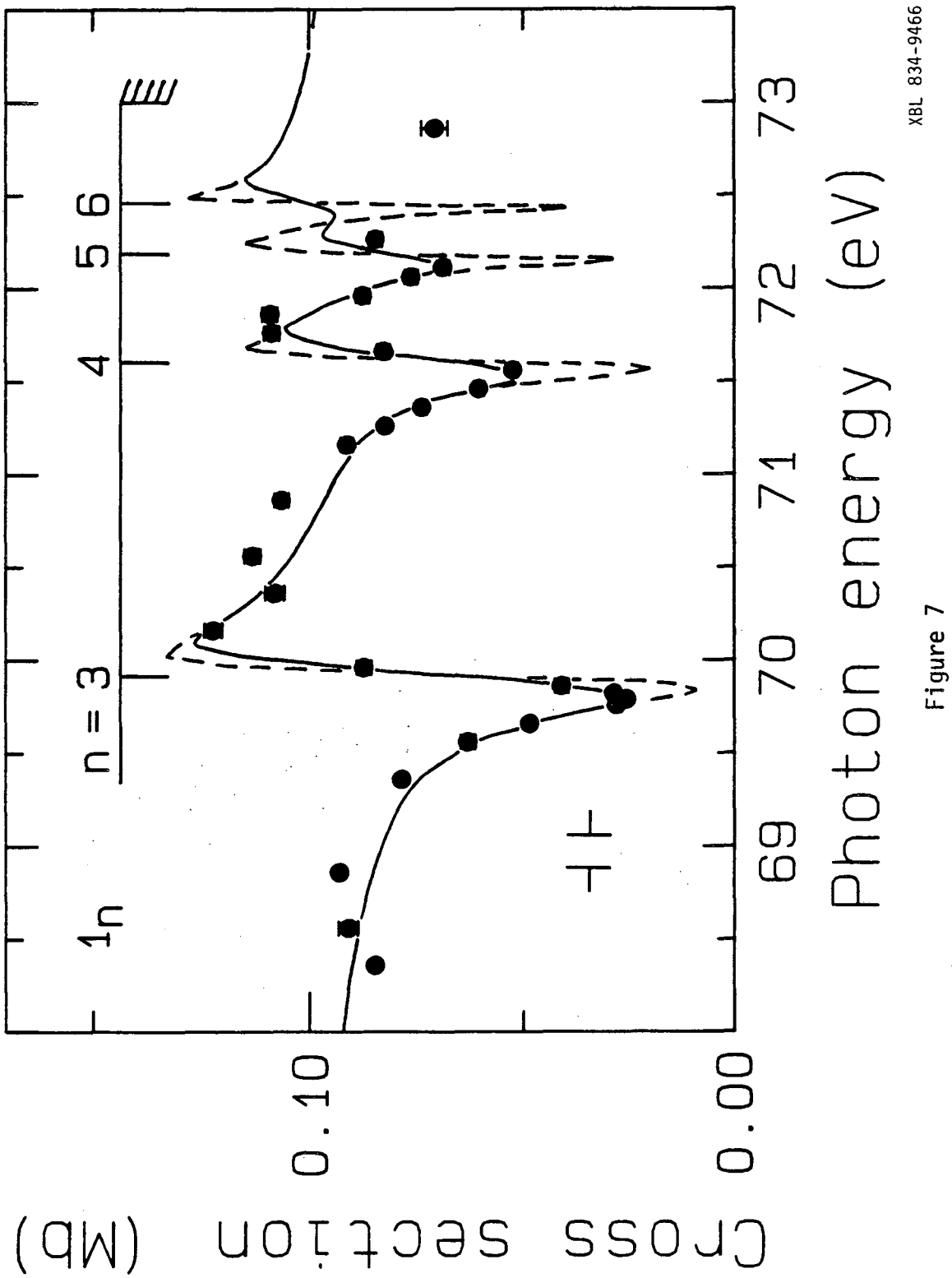


XBL 834-9466

Figure 7

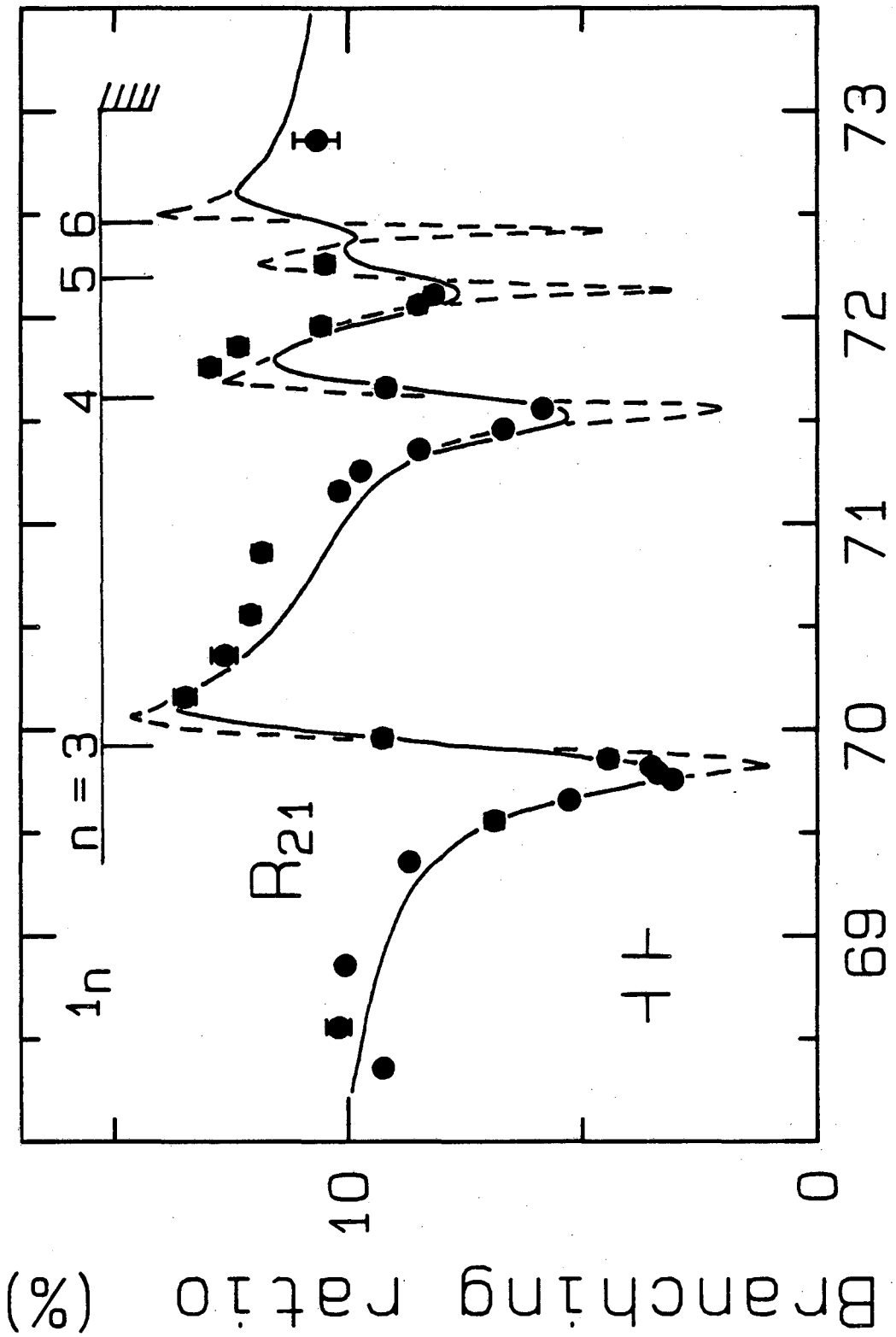


XBL 834-9467

Figure 8

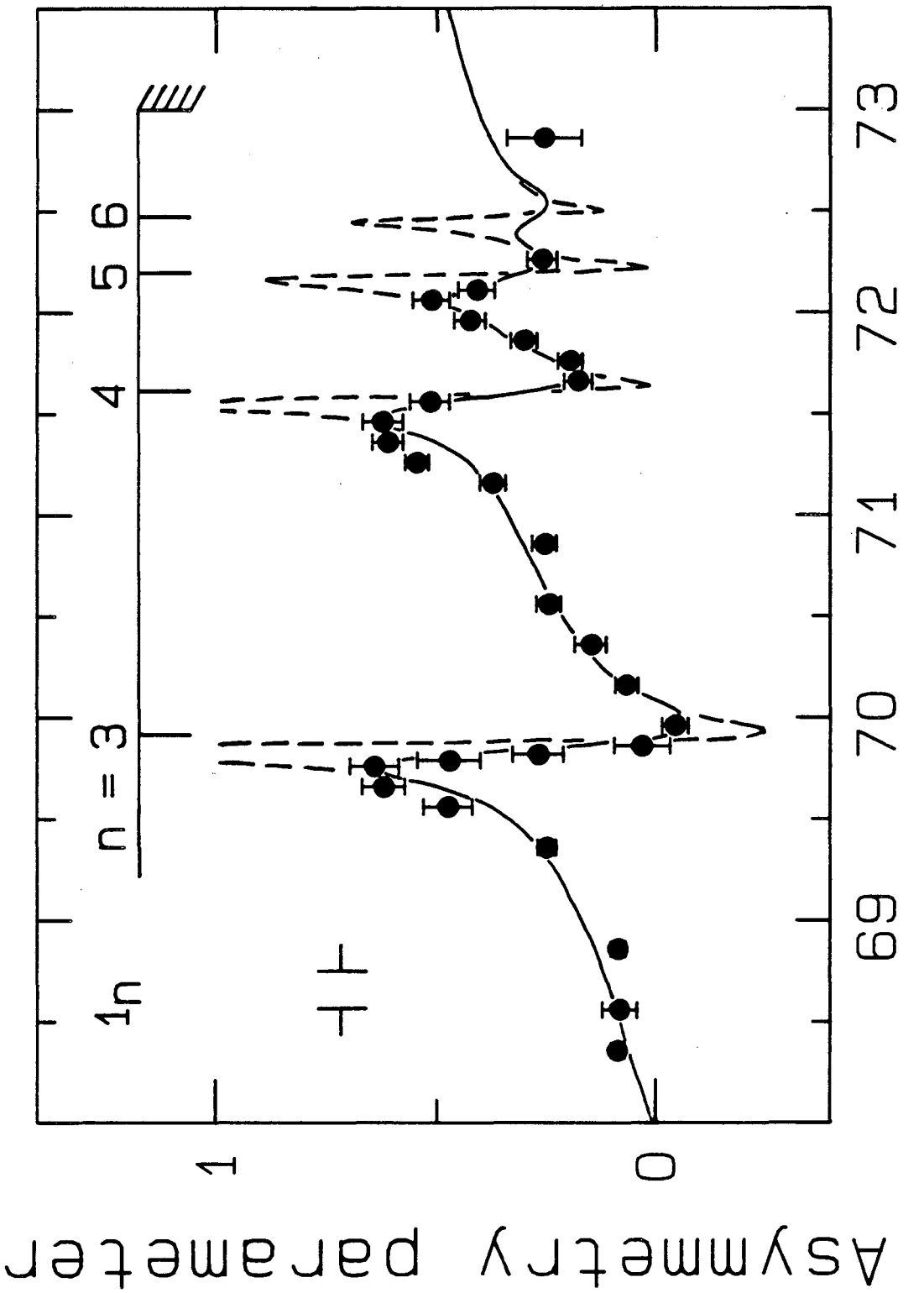


XBL 834-9468

Figure 9

*TECHNICAL INFORMATION DEPARTMENT*
*LAWRENCE BERKELEY LABORATORY*
*UNIVERSITY OF CALIFORNIA*
*BERKELEY, CALIFORNIA 94720*